Sum-Rate Maximization in IRS-Assisted Wireless-Powered Multiuser MIMO Networks With Practical Phase Shift

Ruijin Sun , *Member, IEEE*, Nan Cheng , *Member, IEEE*, Ran Zhang , *Senior Member, IEEE*, Ying Wang , *Member, IEEE*, and Changle Li , *Senior Member, IEEE*

Abstract—The newly emerging intelligent reflecting surface (IRS) with large-scale passive reflecting elements has great potentials to enhance the performance of wireless-powered Internet of Things (IoT) networks, by manipulating the wireless channel. However, most of the existing works considered the ideal reflection of IRS elements with independent amplitude and phase shift. In this article, an IRS-assisted wireless-powered multiuser multi-input–multi-output network is considered, taking into account the practical coupling effect between the reflecting amplitude and the phase shift. Then, an uplink sum-rate maximization problem is investigated by jointly designing the active beamforming of multiple antennas, the passive beamforming of the IRS, and the time allocation ratio. Due to the tightly coupled optimization variables, the formulated problem is nonconvex. To effectively solve this problem, we decompose it into three subproblems, i.e., the active beamforming, the downlink passive beamforming, and the uplink passive beamforming. For the active beamforming design, access point's optimal downlink energy beamforming matrix is proved to be rank-one, and IoT users' optimal uplink information covariance matrices are derived in semi-closed forms. For the downlink passive beamforming design, a low-complexity algorithm based on the successive convex approximation and the penalty function method is proposed. For the uplink passive beamforming design, the multiuser problem is equivalently transformed into a virtual single-user problem, which is solved via an iterative algorithm. Numerical results show that, in comparison with algorithms without IRS, our proposed algorithm can significantly improve the uplink sum rate up to 50% when the number of passive elements is 100.

Index Terms—Intelligent reflecting surface (IRS)-assisted, joint active and passive beamforming, practical phase shift, wireless channel configuration.

Ruijin Sun, Nan Cheng, and Changle Li are with the School of Telecommunications Engineering, Xidian University, Xi'an 710071, China (e-mail: sunruijin@xidian.edu.cn; nancheng@xidian.edu.cn; clli@mail.xidian.edu.cn).

Ran Zhang is with the Department of Electrical and Computer Engineering, Miami University, Oxford, OH 45056 USA (e-mail: zhangran2006@gmail.com).

Ying Wang is with the State Key Laboratory of Networking and Switching Technology, Beijing University of Posts and Telecommunications, Beijing 100876, China (e-mail: wangying@bupt.edu.cn).

I. INTRODUCTION

WITH the rapid development of the smart home and the intelligent city, a new era of Internet of Things (IoT) is flourishing. It has been reported that the number of all types of IoT devices is expected to grow from 6.1 billion in 2018 to 14.7 billion by 2023 [1]. To provide ubiquitous high-quality communications for the massive intelligent IoT devices, massive connectivity and huge data rate are considered as two major drivers for the fifth generation (5G) and beyond. Up to now, IoT devices have been widely applied in various vertical industries, such as health monitoring, building structure sensing, traffic surveillance, and so on. Generally, these IoT devices are powered by embedded batteries, which need to be periodically replaced to prolong the lifetime. However, in some typical scenarios, such as toxic environmental monitoring and embedded monitoring for the health conditions of human bodies, it is impossible or inconvenient to replace the battery, resulting in limited lifetime.

As a promising solution, wireless energy harvesting (EH) enables devices to scavenge the energy from radio frequency (RF) signals sent by the dedicated energy access point (AP). Since the RF electromagnetic wave can concurrently carry the information and the energy, simultaneous wireless information and power transfer (SWIPT) has been widely investigated to characterize the tradeoff between the spectrum efficiency and the EH efficiency [2], [3], [4]. Another related research area is wireless-powered communication networks (WPCNs), where energy-constrained IoT devices are first powered by the AP via downlink and then report their collected data to the AP via uplink by using the harvested energy as the transmission power [5], [6], [7]. Recently, Xiaomi Corporation pronounced that its Mi Air Charge Technology can remotely charge a single phone within several meters, which is realized by a multi-input–multi-output (MIMO) setup with 144 transmitter antennas and 14 receiver antennas [8]. This product exhibition shows the huge potential to apply the large-scale MIMO technology [9] in wireless EH. Although large-scale antenna arrays can significantly improve the EH efficiency leveraging on the beamforming gain, the hardware cost of massive antennas is extremely expensive for widespread practical applications.

Fortunately, intelligent reflecting surface (IRS), best known for its cost effective and easy deployment, has been put forward to combat the wireless channel attenuation and enhance both the information transfer and the EH [10]. Specifically, an

IRS consists of large-scale controllable and low-cost passive elements with each element constituted by a printed dipole and phase shifter. By appropriately adjusting the reflected amplitude and phase shift of each element, referred to as passive beamforming, incident signals can be artificially reflected to desired directions [11]. With such an IRS deployed on the wall, the wireless propagation environment can be reshaped artificially to achieve favorable communication performance. Compared with the traditional active beamforming/relaying, the passive beamforming of IRS without the signal amplification and regeneration consumes lower hardware cost and energy. Due to these compelling benefits, lots of IRS-related research works have been carried out to enlarge the communication coverage [12], maximize the network throughput [13], [14] or improve the amount of harvested energy [15].

A. Prior Related Works

The existing IRS-related works regarding EH include IRS-assisted SWIPT networks and IRS-assisted WPCNs. In typical IRS-assisted SWIPT networks, one AP concurrently serves multiple information decoding (ID) users and EH users via the same RF signals, where IRSs are deployed to optimize the wireless channel. By jointly optimizing the active beamforming of AP and the passive beamforming of IRS, the harvested energy maximization problem and the sum-rate maximization problem were, respectively, investigated in [15] and [16]. In [17], the joint active and passive beamforming was designed to reduce the transmission power with the personalized Quality of Service (QoS) guarantee of both ID and EH users. Different from [15], [16], and [17], a more general nonlinear EH model was considered in IRS-assisted SWIPT networks and the max-min energy efficiency problem was investigated subject to users' individual QoS constraints [18]. All the above works demonstrated that with the help of low-cost IRS, the system performance can be significantly improved, especially in the scenario with weak direct link.

In IRS-assisted WPCNs, a harvest-then-transmit protocol [19] was adopted where energy-constrained users first harvest the RF energy sent by a hybrid AP and then upload their information to the AP by using the harvested energy for the transmission power. Meanwhile, the IRS is deployed to enhance the EH in the downlink and improve the system performance in the uplink. Assuming that both AP and users are equipped with a single antenna, Chu et al. [20] considered that users report their information to AP in a time-division multiple access (TDMA) manner and investigated the joint passive beamforming and time slot allocation problem to maximize the network throughput. To boost the spectrum efficiency, the IRS-assisted WPCN with full-duplex AP was investigated in [21] to maximize the network throughput. Instead of the network throughput, the mean-squared error (MSE) minimization problem was studied in the IRS-aided wireless-powered AirComp network, where the signal superposition in the multiaccess uplink channel was integrated as part of the computation [22]. A further extension was made in [23] by considering an AP with multiple antennas, and the weighted sum-rate maximization problem was investigated by

jointly optimizing the passive beamforming of IRS and the active beamforming of AP.

B. Our Contributions

Although quite a few works have been done in IRS-assisted WPCNs, most of the prior works considered the scenario where the wireless-powered IoT user is equipped with a single antenna. With the miniaturization and integration of the antenna technology, it is possible to equip IoT devices with several antennas [24]. Due to multiple mutually interfered and coupled information flows, existing works on single-antenna IoT users cannot be directly extended to the multiuser MIMO case. Furthermore, although IRS-assisted WPCNs with imperfections have been investigated in the literature, such as beamforming design with imperfect channel state information (CSI) [25] or discrete phase shift [26], all these works considered the ideal phase shift of each IRS element, where the full signal reflecting amplitude and the phase shift are configured independently. In practice, however, there exists a coupling effect between the amplitude response and the phase shift [27], [28]. To fully exploit the potential advantages of multiple active antennas and the large-scale passive antenna array of IRS in practice, in this article, we consider an IRS-aided wireless-powered multiuser MIMO network with the practical phase shift model and investigate the uplink sum-rate maximization problem via the joint optimization of active and passive beamforming. The main contributions are summarized as follows.

1) Different from conventional works on WPCNs without IRS or IRS-assisted WPCNs with single-antenna users and ideal phase shifters, this article considers a general IRS-assisted wireless-powered multiuser MIMO IoT network with the practical phase shift model, where the realistic phase-dependent reflecting amplitude is modeled. The harvest-then-transmit protocol is adopted and each time slot is divided into the downlink energy transfer phase and the uplink data report phase. To understand the potential benefits brought by the multiple active antennas of the transceiver and the large-scale passive antenna array of the IRS, an uplink sum-rate maximization problem is formulated based on the channel reciprocity and the acquired CSI, jointly optimizing the time allocation between the downlink and the uplink phase, the active beamforming matrix of AP, active covariance matrices of IoT users, and passive beamforming matrices of the IRS for the downlink and the uplink.

2) Due to the tightly coupled optimization variables and the nonconvex relationship between the reflecting amplitude and phase shift in each IRS element, the formulated problem is a complicated nonconvex problem. To effectively handle this problem, the original problem is decomposed into three subproblems, i.e., the active beamforming problem, the downlink passive beamforming problem, and the uplink passive beamforming problem, and solved via optimizing these subproblems alternatively. As the downlink passive beamforming

problem and the uplink passive beamforming problem are mutually independent, these two subproblems can be optimized in parallel.

3) For the active beamforming problem, with the Lagrangian method, the optimal rank-one form of AP's downlink energy beamforming matrix and the optimal semi-closed form of each user's uplink information covariance matrix are obtained. For the downlink passive beamforming problem, the formulated feasibility check problem is converted into an optimization problem and solved by a proposed low-complexity algorithm based on the successive convex approximation (SCA) and the penalty function method. For the uplink passive beamforming problem, the multiuser uplink sum-rate maximization problem is equivalently transformed into a virtual single-user rate maximization problem, which can be solved via an iterative algorithm.

4) Extensive numerical results show that IRS with appropriate wireless channel configuration brings remarkable advantage in the considered wireless-powered multiuser MIMO network. The proposed joint active and passive beamforming design can enlarge the uplink sum rate up to 50% compared with the scheme without IRS. Furthermore, it is shown that the better network performance is achieved when the IRS is deployed near the AP or IoT users, which provides a guideline to the practical deployment of the IRS.

The remainder of this article is organized as follows. Section II presents the system model and formulates an uplink sum-rate maximization problem. In Section III, we propose a joint active and passive beamforming design algorithm to iteratively solve the original problem. Extensive numerical results are given in Section IV. Finally, Section V concludes this article.

Notation: Bold lowercase and uppercase letters, respectively, denote column vector and matrix. The superscript $\mathbf{G}^{\mathrm{H}}$ is the (Hermitian) conjugate transpose of $\mathbf{G}$. $\odot$ is the Hadamard product. $\mathrm{Re}\{x\}$ is the real part of complex number x and $[x]_a^+$ means $x \geq a$.

II. SYSTEM MODEL AND PROBLEM FORMULATION

A. System Model

As illustrated in Fig. 1, we consider an IRS-assisted IoT network with one M-antenna AP, one IRS, and K multiple-antenna IoT users. The index set of these IoT users is denoted as $\mathcal{K} = \{1, \ldots, K\}$. IoT user k is equipped with N_k[1] antennas and the total number of antennas of all the IoT users is $N = \sum_{k=1}^{K} N_k$. As IoT users are energy-limited, the considered IoT network operates with a harvest-then-transmit protocol. In particular, IoT users first harvest the RF energy sent by the AP, then report their sensing data to the AP using the harvested energy as the transmission power. To facilitate the EH in the downlink and boost the network capacity in the uplink, one IRS consisting of L passive reflecting elements is deployed

---

[1]The setting of multiple antennas at IoT users is to enhance the EH. To achieve a tradeoff among the EH efficiency, the circuit power consumption, and the cost of IoT users, N_k is set as 2 in the simulation.
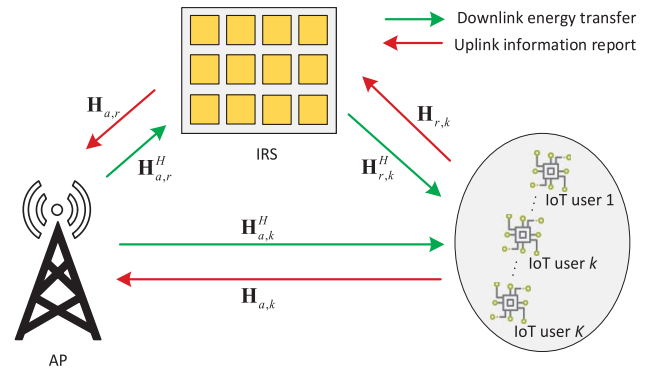

Fig. 1.   IRS-assisted wireless-powered multiuser MIMO network.

in the network. By adjusting the phase shift of each passive reflecting element, the IRS has the ability to configure the wireless channel and reflect the RF signal to the desired direction.

Denote by T the time duration of each harvest-then-transmit slot. The time slot is divided into two parts: $(1 - \tau)T$ for the downlink energy transfer and τT for the uplink data report, where τ is the ratio of data report duration to the whole time slot. Without loss of generality, the time slot T is normalized to be 1 in this article. In the considered scenario, a quasi-static block-fading channel model is adopted, where all channel coefficients almost remain the same in each time slot and independently change from one slot to another. Furthermore, it is assumed that the channel reciprocity holds in our considered IRS-assisted time-division duplex (TDD) systems, which was demonstrated in [29] via practical experiments.

For the CSI acquisition, the direct link between AP and IoT users can be estimated via traditional channel estimation (CE) schemes. Although the CE of IRS-related links is a challenging problem due to the passive nature of the IRS, various effective schemes have been proposed [30]. One workable scheme is installing some dedicated sensing devices with low-power receive RF chains in IRS [31]. With this semi-passive IRS, the channels from the AP/users to the IRS can be separately estimated at these sensing devices based on the pilots sent by the AP/users, and then transmitted to AP via the dedicated control link between AP and IRS. The reverse CSI from the IRS to the AP/users can be acquired by exploiting the channel reciprocity. During the CE, IoT users just transmit a few pilots in the uplink with extremely low power consumption and the energy-consuming CE method is implemented in the AP. In addition, to enhance the EH, IoT users are deployed near the AP or IRS and the signal-to-noise ratio is usually high, which also contributes to the CSI acquisition.

With the acquired CSI, this article mainly characterizes the theoretical performance boundary of IRS-assisted wireless-powered IoT networks. In the following, detailed models in the downlink energy transfer phase and the uplink data report phase are, respectively, given.

1) Downlink Energy Transfer Phase: In the downlink, the AP powers all IoT users via the active transmit beamforming of AP and the passive reflect beamforming of IRS. The downlink energy signal for IoT user k is denoted as

$s_{d,k}$, which independently follows arbitrary distribution with $\mathbb{E}(|s_{d,k}|^2) = 1$. Then, the transmitted energy signal sent by AP is expressed as

$$x_d = \sum_{k=1}^{K} \boldsymbol{w}_k s_{d,k} \tag{1}$$

where $\boldsymbol{w}_k \in \mathbb{C}^{M \times 1}$ is the active transmit beam for IoT user k.

With the assistance of the IRS, the wireless channel in the considered scenario consists of both the direct AP–user link and the indirect AP–IRS–user link (i.e., IRS-assisted link). Let $\boldsymbol{H}_{a,k}^{\mathrm{H}} \in \mathbb{C}^{N_k \times M}$, $\boldsymbol{H}_{a,r}^{\mathrm{H}} \in \mathbb{C}^{L \times M}$, and $\boldsymbol{H}_{r,k}^{\mathrm{H}} \in \mathbb{C}^{N_k \times L}$ denote the equivalent baseband channel matrices from AP to IoT user k, from AP to IRS, and from IRS to IoT user k, respectively. In the IRS-assisted link, by jointly adjusting the phase shift and/or amplitude of L reflecting elements embedded in IRS, the incident signal can be scattered to the desired direction with controllable power strength. Define $\boldsymbol{f}_d = [f_{d,1}, \ldots, f_{d,L}]^T$ with $f_{d,l} = \beta_{d,l} e^{j\theta_{d,l}}$ as the downlink reflecting vector of the IRS, where $f_{d,l}$, $\theta_{d,l} \in [-\pi, \pi]$ and $\beta_{d,l} \in [0, 1]$, respectively, denote the reflecting coefficient, the phase shift, and the amplitude of passive reflecting element l in the downlink. As a result, the downlink IRS-assisted link from AP to IoT user k is modeled as $\boldsymbol{H}_{r,k}^{\mathrm{H}} \boldsymbol{F}_d \boldsymbol{H}_{a,r}^{\mathrm{H}} \in \mathbb{C}^{M \times 1}$, where $\boldsymbol{F}_d = \mathrm{diag}(\boldsymbol{f}_d)$ is the downlink reflecting matrix of the IRS. Notice that $\boldsymbol{f}_d$ can be regarded as the passive reflect beam of the IRS being optimized to enhance the EH.

The energy signal received by IoT user k is given as

$$y_k = \left(\boldsymbol{H}_{a,k}^{\mathrm{H}} + \boldsymbol{H}_{r,k}^{\mathrm{H}} \boldsymbol{F}_d \boldsymbol{H}_{a,r}^{\mathrm{H}}\right)\left(\sum_{i=1}^{K} \boldsymbol{w}_i s_{d,i}\right) + \boldsymbol{n}_k \tag{2}$$

where $\boldsymbol{n}_k \sim \mathcal{CN}(\boldsymbol{0}, \sigma_k^2 \boldsymbol{I}_{N_k})$ is the additive white Gaussian noise (AWGN) vector received by IoT user k with σ_k^2 being the noise power. Let $\boldsymbol{G}_{d,k}^{\mathrm{H}} = \boldsymbol{H}_{a,k}^{\mathrm{H}} + \boldsymbol{H}_{r,k}^{\mathrm{H}} \boldsymbol{F}_d \boldsymbol{H}_{a,r}^{\mathrm{H}}$ denote the composite downlink channel from AP to IoT user k, the harvested energy of IoT user k is then represented as

$$\begin{aligned} E_k &= \sum_{i=1}^{K} (1-\tau)\rho_k \left\| \left(\boldsymbol{H}_{a,k}^{\mathrm{H}} + \boldsymbol{H}_{r,k}^{\mathrm{H}} \boldsymbol{F}_d \boldsymbol{H}_{a,r}^{\mathrm{H}}\right)\boldsymbol{w}_i \right\|_2^2 \\ &= (1-\tau)\rho_k \mathrm{Tr}\left(\boldsymbol{G}_{d,k}^{\mathrm{H}} \boldsymbol{W} \boldsymbol{G}_{d,k}\right) \end{aligned} \tag{3}$$

where $\boldsymbol{W} = \sum_{i=1}^{K} \boldsymbol{w}_i \boldsymbol{w}_i^{\mathrm{H}}$ and $\rho_k \in (0, 1)$ is the energy conversion efficiency of IoT user k.[2]

2) Uplink Data Report Phase: In the uplink, all IoT users report their sensing data to the AP simultaneously. The information signal transmitted by IoT user k is denoted as $\boldsymbol{s}_{u,k} \in \mathbb{C}^{N_k \times 1}$, which is a complex Gaussian random vector with zero mean and covariance matrix $\boldsymbol{S}_k \succeq \boldsymbol{0}$, i.e.,

---

[2]Despite the fact that the nonlinear EH model can better fit the case where the input power level is above the saturation threshold, the linear EH model is also accurate for most practical EH circuits operating in a large range of input RF power [32]. Benefiting from the accuracy for most EH circuits in practical deployment and the simple mathematical property, the linear EH model has been widely used in the literature for the resource allocation. Thus, in this article, we adopt the linear EH model. Notice that our proposed algorithm cannot be directly applied to the nonlinear EH model, which requires a dedicated study and we will do it in the future.

$\boldsymbol{s}_{u,k} \sim \mathcal{CN}(\boldsymbol{0}, \boldsymbol{S}_k)$. The received information signal at AP is expressed as

$$\boldsymbol{y}_a = \sum_{k=1}^{K} (\boldsymbol{H}_{a,k} + \boldsymbol{H}_{a,r} \boldsymbol{F}_u \boldsymbol{H}_{r,k}) \boldsymbol{s}_{u,k} + \boldsymbol{n}_a \tag{4}$$

where $\boldsymbol{n}_a \sim \mathcal{CN}(\boldsymbol{0}, \sigma_a^2 \boldsymbol{I}_M)$ is the AWGN vector received by AP with σ_a^2 being the noise power, and $\boldsymbol{F}_u$ is the uplink reflecting matrix. To be specific, $\boldsymbol{F}_u = \mathrm{diag}(\boldsymbol{f}_u)$ with $\boldsymbol{f}_u = [f_{u,1}, \ldots, f_{u,L}]^T$ and $f_{u,l} = \beta_{u,l} e^{j\theta_{u,l}}$, where $f_{u,l}$, $\theta_{u,l}$ and $\beta_{u,l}$, respectively, denote the reflecting coefficient, the phase shift, and the amplitude of reflecting element l in the uplink.

According to [33], the achievable uplink sum rate of all IoT users is represented as

$$C = \tau \log_2\left(\det\left(\boldsymbol{I} + \frac{1}{\sigma_a^2} \sum_{k=1}^{K} \boldsymbol{G}_{u,k} \boldsymbol{S}_k \boldsymbol{G}_{u,k}^{\mathrm{H}}\right)\right) \tag{5}$$

where $\boldsymbol{G}_{u,k} = \boldsymbol{H}_{a,k} + \boldsymbol{H}_{a,r} \boldsymbol{F}_u \boldsymbol{H}_{r,k}$ is the composite uplink channel from IoT user k to AP. This uplink sum rate can be achieved by the minimum mean-square error (MMSE) receiver at AP with the successive interference cancellation (SIC) [33]. It is worth pointing out that the achievable uplink sum rate considered in this article, i.e., (5), is the channel capacity of the uplink multiuser scenario, which is an upper bound of the sum rate in IoT networks.

Remark 1: For the finite block-length transmission in IoT networks, according to [34], the achievable rate is expressed as $R(\gamma; n, \epsilon) = C(\gamma) - \sqrt{(V/n)} Q^{-1}(\epsilon)$, where $C(\gamma)$ is the channel capacity with γ representing the signal-to-noise ratio, n is the block length, ϵ is the error probability, Q is the complementary Gaussian cumulative distribution function, and V is a characteristic of the channel referred to as channel dispersion. In particular, V is given by $V = 1 - (1/[(1+\gamma)^2])$. It can be observed that V is an increasing function with respect to γ and satisfies $0 \leq V < 1$. If we approximate V by 1, the rate with finite block-length transmission $R(\gamma; n, \epsilon)$ is simplified as $\bar{R}(\gamma; n, \epsilon) = C(\gamma) - Q^{-1}(\epsilon)/\sqrt{n}$, which is a lower bound of $R(\gamma; n, \epsilon)$. As $V \approx 1$ when $\gamma \geq 5$ dB [35], this lower bound is tight in high SNR regions. For the case with $\gamma < 5$ dB, the achievable rate with finite-block transmission $R(\gamma; n, \epsilon)$ is much higher than $\bar{R}(\gamma; n, \epsilon)$. Mathematically, we have

$$\begin{cases} \bar{R}(\gamma; n, \epsilon) \approx R(\gamma; n, \epsilon) < C(\gamma), & \gamma \geq 5 \text{ dB} \\ \bar{R}(\gamma; n, \epsilon) < R(\gamma; n, \epsilon) < C(\gamma), & \gamma < 5 \text{ dB}. \end{cases} \tag{6}$$

In this article, therefore, with the channel capacity C achieved by (5) and the lower bound $\bar{R}(\gamma; n, \epsilon)$ obtained by $C - Q^{-1}(\epsilon)/\sqrt{n}$, the value range of the achievable rate with finite block-length transmission $R(\gamma; n, \epsilon)$ can be determined. Besides, $R(\gamma; n, \epsilon)$ gradually approaches to its lower bound $\bar{R}(\gamma; n, \epsilon)$ with the increase of γ.

B. Practical Phase Shift Model of the IRS

For the phase shift of the IRS, most of the existing works separately model the reflecting amplitude and the phase shift of each IRS element, where the reflecting amplitude is always setting as 1 and only the phase shift is flexibly adjusted. To

figure out the practical signal reflecting model of each IRS element, [27] deeply analyzes the reflecting principle of the IRS and finds that the reflecting amplitude and the phase shift are controlled by the semiconductor device with tunable impedance. Then, via the equivalent circuit model of the reflecting unit cell, [27] reveals the relationship curve between the reflecting amplitude and the phase shift, which is also verified via practical experiments. This phenomenon shows that the reflecting amplitude of each IRS element is a function of its phase shift in reality.

To mathematically characterize this function, [28] further proposes an analytical model for the IRS reflection. In specific, the reflecting coefficient of the lth unit in IRS is expressed as

$$f_l = \beta_l(\theta_l) e^{j\theta_l} \tag{7}$$

where

$$\beta_l(\theta_l) = (1 - \beta_{\min}) \left(\frac{\sin(\theta_l - \bar{\theta}) + 1}{2} \right)^\chi + \beta_{\min} \in [0, 1] \tag{8}$$

denotes the reflecting amplitude and $\theta_l \in [-\pi, \pi)$ is the phase shift. In the expression of (8), $\beta_{\min} \geq 0$, $\bar{\theta} \geq 0$ and $\chi \geq 0$ are the constants related to the specific circuit implementation and can be obtained via the curve fitting method. With this practical model, the downlink and uplink reflecting coefficients of IRS element l are, respectively, represented as

$$f_{d,l} = \beta_{d,l} e^{j\theta_{d,l}} = \beta_l(\theta_{d,l}) e^{j\theta_{d,l}} \text{ and} \tag{9}$$

$$f_{u,l} = \beta_{u,l} e^{j\theta_{u,l}} = \beta_l(\theta_{u,l}) e^{j\theta_{u,l}}. \tag{10}$$

C. Problem Formulation

With the considered IRS-assisted wireless-powered multiuser MIMO network, we aim to maximize the achievable uplink sum rate of all IoT users by jointly optimizing the time allocation ratio, downlink active beamforming of AP, the uplink active information covariance matrices of all IoT users, and the passive beamforming of IRS for both the downlink and uplink. Mathematically, the problem is formulated as

$$\mathcal{P}1: \max_{\substack{\tau, W, F_d, \\ F_u, S}} \quad \tau \log_2 \left(\det \left(I + \frac{1}{\sigma_a^2} \sum_{k=1}^K G_{u,k} S_k G_{u,k}^H \right) \right) \tag{11a}$$

$$\text{s.t.} \quad \text{Tr}(W) \leq P_a \tag{11b}$$

$$\tau \text{Tr}(S_k) \leq (1 - \tau) \rho_k \text{Tr}(G_{d,k}^H W G_{d,k}) \ \forall k \tag{11c}$$

$$f_{d,l} = \beta_l(\theta_{d,l}) e^{j\theta_{d,l}}, \ \theta_{d,l} \in [-\pi, \pi) \ \forall l \tag{11d}$$

$$f_{u,l} = \beta_l(\theta_{u,l}) e^{j\theta_{u,l}}, \ \theta_{u,l} \in [-\pi, \pi) \ \forall l \tag{11e}$$

$$0 < \tau < 1, W \succeq 0, S_k \succeq 0 \ \forall k \tag{11f}$$

where $S = [S_1, \ldots, S_K]$ and P_a is the maximum allowable transmission power of AP. Constraint (11b) is the transmission power constraint of AP and (11c) is the energy causality constraint, which ensures that the consumed energy of each IoT user in the uplink is no more than its harvested energy in the downlink. Constraints (11d) and (11e) are, respectively, the practical IRS reflection constraints for the downlink and uplink transmission.

Notice that problem $\mathcal{P}1$ is nonconvex due to the tightly coupled time allocation ratio, active beamforming and passive beamforming in objective function (11a) and the energy causality constraint (11c), as well as the nonconvexity of IRS reflection constraints (11d) and (11e). To tackle this complicated problem effectively, in Section III, we divide the optimization variables into three blocks and update them alternatively.

III. PROPOSED JOINT ACTIVE AND PASSIVE BEAMFORMING DESIGN

In this section, we present the proposed joint active and passive beamforming design to tackle the formulated uplink sum-rate maximization problem $\mathcal{P}1$. In particular, problem $\mathcal{P}1$ is decomposed into three subproblems, i.e., the active beamforming problem with the optimization of $\{W, S, \tau\}$, the downlink passive beamforming problem with the optimization of F_d, and the uplink passive beamforming problem with the optimization of F_u. In what follows, specific solutions to these three subproblems and the overall algorithm for solving problem $\mathcal{P}1$ are, respectively, given.

A. Active Beamforming: Fix $\{F_d, F_u\}$ and Optimize $\{W, S, \tau\}$

With any given channel configuration F_d and F_u, the original problem $\mathcal{P}1$ is reduced as the active beamforming problem $\mathcal{P}2$ with optimization variables W, S, and τ, which is cast as

$$\mathcal{P}2: \max_{W, S, \tau} \quad \tau \log_2 \left(\det \left(I + \frac{1}{\sigma_a^2} \sum_{k=1}^K G_{u,k} S_k G_{u,k}^H \right) \right) \tag{12a}$$

$$\text{s.t.} \quad \text{Tr}(W) \leq P_a \tag{12b}$$

$$\tau \text{Tr}(S_k) \leq (1 - \tau) \rho_k \text{Tr}(G_{d,k}^H W G_{d,k}) \ \forall k \tag{12c}$$

$$W \succeq 0, S_k \succeq 0 \ \forall k. \tag{12d}$$

Due to the coupling of τ and W in (12a) as well as the coupling of τ and S_k in (12c), problem $\mathcal{P}2$ is nonconvex.

To tackle this obstacle, we introduce two new variables $\tilde{W} = (1 - \tau)W$ and $\tilde{S}_k = \tau S_k$, and problem $\mathcal{P}2$ is then equivalently recast as

$$\mathcal{P}3: \max_{\tilde{W}, \tilde{S}, \tau} \quad \tau \log_2 \left(\det \left(I + \frac{1}{\sigma_a^2 \tau} \sum_{k=1}^K G_{u,k} \tilde{S}_k G_{u,k}^H \right) \right) \tag{13a}$$

$$\text{s.t.} \quad \text{Tr}\left(\tilde{W} \right) \leq (1 - \tau) P_a \tag{13b}$$

$$\text{Tr}\left(\tilde{S}_k \right) \leq \rho_k \text{Tr}\left(G_{d,k}^H \tilde{W} G_{d,k} \right) \ \forall k \tag{13c}$$

$$0 < \tau < 1, \tilde{W} \succeq 0, \tilde{S}_k \succeq 0 \ \forall k. \tag{13d}$$

Notice that the objective function (13a) is the perspective of the concave function $\log_2(\det(I + (1/\sigma_a^2) \sum_{k=1}^K G_{u,k} \tilde{S}_k G_{u,k}^H))$. According to [36], the concavity is preserved by the perspective operation, (13a) is hence joint concave with respect to $\tilde{S}_k$ and τ. Furthermore, all constraints in problem $\mathcal{P}3$ are convex. Therefore, problem $\mathcal{P}3$ is a convex optimization problem and can be optimally solved by CVX. However, the general solver is usually accompanied by the high computational complexity. In this article, we propose a low-complexity

algorithm based on the Lagrangian method and the Karush–Kuhn–Tucker (KKT) condition to obtain the optimal solution to problem $\mathcal{P}3$.

1) Overview of the Proposed Active Beamforming Design: Denote $\alpha \geq 0$, $\beta_k \geq 0$, $\boldsymbol{\Psi}_w \succeq \mathbf{0}$, and $\boldsymbol{\Psi}_{s,k} \succeq \mathbf{0}$ as Lagrangian multipliers associated with (12b), (12c), $\boldsymbol{W} \succeq \mathbf{0}$, and $\boldsymbol{S}_k \succeq \mathbf{0}$, respectively. Define $\boldsymbol{\beta} = [\beta_1, \ldots, \beta_K]^T$ and $\boldsymbol{\Psi}_s = [\boldsymbol{\Psi}_{s,1}, \ldots, \boldsymbol{\Psi}_{s,K}]$, the Lagrangian function of problem $\mathcal{P}3$ is expressed as

$$\mathcal{L}\left(\tilde{\boldsymbol{W}}, \tilde{\boldsymbol{S}}, \tau; \alpha, \boldsymbol{\beta}, \boldsymbol{\Psi}_w, \boldsymbol{\Psi}_s\right)$$
$$= \tau \log_2\left(\det\left(\boldsymbol{I} + \frac{1}{\sigma_a^2 \tau} \sum_{k=1}^{K} \boldsymbol{G}_{u,k} \tilde{\boldsymbol{S}}_k \boldsymbol{G}_{u,k}^{\mathrm{H}}\right)\right) + \mathrm{Tr}\left(\boldsymbol{A}\tilde{\boldsymbol{W}}\right)$$
$$+ \sum_{k=1}^{K} \mathrm{Tr}\left(\boldsymbol{B}_k \tilde{\boldsymbol{S}}_k\right) + (1 - \tau)\alpha P_a \qquad (14)$$

where

$$\boldsymbol{A} = \sum_{k=1}^{K} \beta_k \rho_k \boldsymbol{G}_{d,k} \boldsymbol{G}_{d,k}^{\mathrm{H}} + \boldsymbol{\Psi}_w - \alpha \boldsymbol{I} \qquad (15)$$
$$\boldsymbol{B}_k = -\beta_k \boldsymbol{I} + \boldsymbol{\Psi}_{s,k}. \qquad (16)$$

Then, the Lagrangian dual function is given as

$$\mathcal{P}4 : \mathcal{D}(\alpha, \boldsymbol{\beta}, \boldsymbol{\Psi}_w, \boldsymbol{\Psi}_s) = \max_{\tilde{\boldsymbol{W}}, \tilde{\boldsymbol{S}}, \tau} \mathcal{L}\left(\tilde{\boldsymbol{W}}, \tilde{\boldsymbol{S}}, \tau; \alpha, \boldsymbol{\beta}, \boldsymbol{\Psi}_w, \boldsymbol{\Psi}_s\right).$$
$$(17)$$

Since problem $\mathcal{P}3$ is convex and satisfies Slater's condition, the strong duality holds. Thus, the optimal solution to problem $\mathcal{P}3$ can be achieved via its Lagrangian dual problem, which is formulated as

$$\mathcal{P}5: \min_{\alpha, \boldsymbol{\beta}, \boldsymbol{\Psi}_w, \boldsymbol{\Psi}_s} \mathcal{D}(\alpha, \boldsymbol{\beta}, \boldsymbol{\Psi}_w, \boldsymbol{\Psi}_s) \qquad (18a)$$
$$\text{s.t. } \alpha \geq 0, \beta_k \geq 0, \boldsymbol{\Psi}_w \succeq \mathbf{0}, \boldsymbol{\Psi}_{s,k} \succeq \mathbf{0} \ \forall k.$$
$$(18b)$$

As it is extremely difficult to obtain the analytical expression of the Lagrangian dual function $\mathcal{D}(\alpha, \boldsymbol{\beta}, \boldsymbol{\Psi}_w, \boldsymbol{\Psi}_s)$, we optimize problem $\mathcal{P}3$ via alternatively updating primal variables $\{\tilde{\boldsymbol{W}}, \tilde{\boldsymbol{S}}, \tau\}$ and Lagrangian multipliers $\{\alpha, \boldsymbol{\beta}, \boldsymbol{\Psi}_w, \boldsymbol{\Psi}_s\}$. In specific, due to the independence from each other, $\tilde{\boldsymbol{W}}$ and $\{\tilde{\boldsymbol{S}}, \tau\}$ can be optimized in parallel when solving problem $\mathcal{P}4$. During this, the optimal rank-one $\tilde{\boldsymbol{W}}$ with closed-form expression is derived and the special structure of each optimal $\tilde{\boldsymbol{S}}_k$ with semi-closed form is also achieved. Then, Lagrangian multipliers are updated by handling problem $\mathcal{P}5$. With the obtained optimal $\{\tilde{\boldsymbol{W}}, \tilde{\boldsymbol{S}}, \tau\}$, the optimal solution to problem $\mathcal{P}2$ is derived as $\boldsymbol{W} = \tilde{\boldsymbol{W}}/(1 - \tau)$ and $\boldsymbol{S}_k = \tilde{\boldsymbol{S}}_k/\tau$. The detailed active beamforming design is summarized in Algorithm 1. In the following, the update of $\tilde{\boldsymbol{W}}$, $\{\tilde{\boldsymbol{S}}, \tau\}$, and $\{\alpha, \boldsymbol{\beta}, \boldsymbol{\Psi}_w, \boldsymbol{\Psi}_s\}$ is, respectively, introduced.

2) Fix $\{\alpha, \boldsymbol{\beta}, \boldsymbol{\Psi}_w, \boldsymbol{\Psi}_s\}$ and Optimize $\tilde{\boldsymbol{W}}$: In this article, the optimal $\tilde{\boldsymbol{W}}$ with closed-form expression is obtained based on the KKT condition. To show this, we first derive the KKT conditions of problem $\mathcal{P}3$ associated with $\tilde{\boldsymbol{W}}$. Taking the first-order derivation of the Lagrangian function (14) with respect

---

Algorithm 1 Active Beamforming Design to Maximize the Uplink Sum Rate

---
1: Initialize Lagrangian multiplier vector $\boldsymbol{\beta}$ and all users' aggregated uplink information covariance matrix $\tilde{\boldsymbol{S}}$;
2: Calculate Lagrangian multipliers α, $\boldsymbol{\Psi}_w$ and $\boldsymbol{\Psi}_s$ based on (33), (20) and (25), respectively;
3: **while** The stopping criteria is not satisfied **do**
4:     Update $\tilde{\boldsymbol{W}}$ according to ***Proposition 1***;
5:     **while** The stopping criteria is not satisfied **do**
6:        Update each $\tilde{\boldsymbol{S}}_k$ with any given $\{\tilde{\boldsymbol{S}}_i, i \neq k\}$ according to ***Proposition 2***;
7:        Update τ via the bisection method to solve (30);
8:     **end while**
9:     Update Lagrangian multipliers $\boldsymbol{\beta}$, α, $\boldsymbol{\Psi}_w$ and $\boldsymbol{\Psi}_s$ based on (32), (33), (20) and (25), respectively;
10: **end while**
11: **return** $\boldsymbol{W} = \tilde{\boldsymbol{W}}/(1 - \tau)$ and $\boldsymbol{S} = \tilde{\boldsymbol{S}}/\tau$.

---

to $\tilde{\boldsymbol{W}}$, we have

$$\frac{\partial \mathcal{L}}{\partial \tilde{\boldsymbol{W}}} = \sum_{k=1}^{K} \beta_k \rho_k \boldsymbol{G}_{d,k} \boldsymbol{G}_{d,k}^{\mathrm{H}} - \alpha \boldsymbol{I} + \boldsymbol{\Psi}_w = \mathbf{0}. \qquad (19)$$

Then, the $\tilde{\boldsymbol{W}}$-related KKT conditions are given as

$$\boldsymbol{\Psi}_w = \alpha \boldsymbol{I} - \sum_{k=1}^{K} \beta_k \rho_k \boldsymbol{G}_{d,k} \boldsymbol{G}_{d,k}^{\mathrm{H}} \qquad (20)$$
$$\mathrm{Tr}\left(\boldsymbol{\Psi}_w \tilde{\boldsymbol{W}}\right) = 0 \qquad (21)$$
$$\boldsymbol{\Psi}_w \succeq \mathbf{0}, \tilde{\boldsymbol{W}} \succeq \mathbf{0} \qquad (22)$$

where (21) is the complementary slackness condition.

Proposition 1: The optimal active energy beamforming matrix $\tilde{\boldsymbol{W}}$ satisfies $\mathrm{Rank}(\tilde{\boldsymbol{W}}) = 1$ and has the following structure $\tilde{\boldsymbol{W}} = P_a \boldsymbol{\pi} \boldsymbol{\pi}^{\mathrm{H}}$, where $\boldsymbol{\pi}$ is the unit-norm eigenvector corresponding to the maximum eigenvalue of matrix $\boldsymbol{C} = \sum_{k=1}^{K} \beta_k \rho_k \boldsymbol{G}_{d,k} \boldsymbol{G}_{d,k}^{\mathrm{H}}$.

Proof: We first prove the rank-one property of matrix $\tilde{\boldsymbol{W}}$ via its associated KKT conditions. In KKT conditions, the complementary slackness condition $\mathrm{Tr}(\boldsymbol{\Psi}_w \tilde{\boldsymbol{W}}) = 0$ is equivalent to $\boldsymbol{\Psi}_w \tilde{\boldsymbol{W}} = \mathbf{0}$, since both $\boldsymbol{\Psi}_w$ and $\tilde{\boldsymbol{W}}$ are nonnegative matrices. $\boldsymbol{\Psi}_w \tilde{\boldsymbol{W}} = \mathbf{0}$ means that the optimal active energy beamforming matrix $\tilde{\boldsymbol{W}}$ lies in the null space of $\boldsymbol{\Psi}_w$ and $\mathrm{Rank}(\boldsymbol{\Psi}_w) + \mathrm{Rank}(\tilde{\boldsymbol{W}}) \leq M$.

With $\boldsymbol{C} = \sum_{k=1}^{K} \beta_k \rho_k \boldsymbol{G}_{d,k} \boldsymbol{G}_{d,k}^{\mathrm{H}}$, the Lagrangian multiplier $\boldsymbol{\Psi}_w$ can be rewritten as $\boldsymbol{\Psi}_w = \alpha \boldsymbol{I} - \boldsymbol{C}$ according to (20). Let $\eta_{\max}$ represent the maximum eigenvalue of $\boldsymbol{C}$ and then $\alpha - \eta_{\max}$ is the minimum eigenvalue of $\boldsymbol{\Psi}_w$. Since $\boldsymbol{\Psi}_w$ is a nonnegative matrix, $\alpha \geq \eta_{\max}$ needs to be satisfied. If $\alpha > \eta_{\max}$, $\boldsymbol{\Psi}_w$ is a full-rank matrix. Considering $\mathrm{Rank}(\boldsymbol{\Psi}_w) + \mathrm{Rank}(\tilde{\boldsymbol{W}}) \leq M$, the energy beamforming matrix $\tilde{\boldsymbol{W}} = \mathbf{0}$, which is obviously not the optimal case. Therefore, at the optimum, $\alpha = \eta_{\max}$ must hold. Furthermore, owing to the randomness of the wireless channel, the probability that multiple eigenvalues of $\boldsymbol{C}$ equal to $\eta_{\max}$ approaches to zero. This leads to $\mathrm{Rank}(\boldsymbol{\Psi}_w) = M - 1$.

Based on the fact that $\boldsymbol{\Psi}_w \tilde{\boldsymbol{W}} = \mathbf{0}$ and $\mathrm{Rank}(\boldsymbol{\Psi}_w) = M - 1$, we have $\mathrm{Rank}(\tilde{\boldsymbol{W}}) = 1$ and the optimal rank-one energy

beamforming matrix $\tilde{W}$ can be constructed as

$$\tilde{W} = P_a \boldsymbol{\pi} \boldsymbol{\pi}^{\mathrm{H}} \tag{23}$$

where $\boldsymbol{\pi}$ is a unit-norm vector within the null space of $\boldsymbol{\Psi}_w$. According to the matrix theory, one can verify that $\boldsymbol{\pi}$ is also the eigenvector corresponding to the maximum eigenvalue $\eta_{\max}$ of matrix $\boldsymbol{C}$. This completes the proof. ∎

3) Fix {α, $\boldsymbol{\beta}$, $\boldsymbol{\Psi}_w$, $\boldsymbol{\Psi}_s$} and Optimize {$\tilde{S}$, τ}: To investigate the structure of each $\tilde{S}_k$ with any given τ, we first get the key inspiration from the KKT condition and then propose an optimal iterative algorithm to handle problem $\mathcal{P}4$. Toward this end, taking the first derivation of Lagrangian function (14) with respect to $\tilde{S}_k$, we have

$$\frac{\partial \mathcal{L}}{\partial \tilde{S}_k} = \frac{1}{\sigma_a^2 \ln 2} G_{u,k}^{\mathrm{H}} \left(I + \sum_{i=1}^{K} \frac{1}{\sigma_a^2 \tau} G_{u,i} \tilde{S}_i G_{u,i}^{\mathrm{H}} \right)^{-1} G_{u,k}$$
$$- \beta_k I + \boldsymbol{\Psi}_{s,k} = \boldsymbol{0} \tag{24}$$

which is derived based on $\nabla \ln \det(\boldsymbol{I} + \boldsymbol{G}\boldsymbol{S}\boldsymbol{G}^{\mathrm{H}}) = \boldsymbol{G}^{\mathrm{H}}(\boldsymbol{I} + \boldsymbol{G}\boldsymbol{S}\boldsymbol{G}^{\mathrm{H}})^{-1}\boldsymbol{G}$. Then, the $\tilde{S}_k$-related KKT conditions consisting of $\partial \mathcal{L}/\partial \tilde{S}_k = \boldsymbol{0}$, complementary slackness conditions, primal constraints, and dual constraints are expressed as

$$\beta_k I = \frac{1}{\sigma_a^2 \ln 2} G_{u,k}^{\mathrm{H}} \left(I + \sum_{i=1}^{K} \frac{1}{\sigma_a^2 \tau} G_{u,i} \tilde{S}_i G_{u,i}^{\mathrm{H}} \right)^{-1} G_{u,k}$$
$$+ \boldsymbol{\Psi}_{s,k} \ \forall k \tag{25}$$

$$\mathrm{Tr}\left(\boldsymbol{\Psi}_{s,k} \tilde{S}_k \right) = 0 \ \forall k \tag{26}$$

$$\boldsymbol{\Psi}_{s,k} \succeq \boldsymbol{0}, \tilde{S}_k \succeq \boldsymbol{0} \ \forall k. \tag{27}$$

Notice that the solution to the single-user problem with $K = 1$ also exactly satisfies the KKT condition above. It is instructive to compare the single-user KKT condition with the multiuser KKT condition for each user k. The only difference is that the multiuser KKT condition has the additional background interference term $\boldsymbol{I}_{b,k} = \sum_{i=1, i \neq k}^{K} \boldsymbol{G}_{u,i} \tilde{S}_i \boldsymbol{G}_{u,i}^{\mathrm{H}}/(\sigma_a^2 \tau)$ in (25). Inspired by this observation, if each $\tilde{S}_k$ satisfies the single-user KKT condition while treating other users' signal $\boldsymbol{I}_{b,k}$ as interference, the aggregated matrix $\tilde{S}$ must meet the multiuser KKT condition. Due to the sufficiency of the KKT condition, the obtained $\tilde{S}$ is also the optimal solution to the multiuser problem.

Motivated by this observation, an iterative algorithm is proposed in this article to find the optimal $\tilde{S}$ by solving problem $\mathcal{P}4$. The key idea is to alternatively optimize each $\tilde{S}_k$ with any given $\boldsymbol{I}_{b,k}$ obtained from the previous iteration. To proceed with, in each iteration, the $\tilde{S}_k$ optimization within problem $\mathcal{P}4$ is reduced as

$$\mathcal{P}6 : \max_{\tilde{S}_k} \ \log_2 \left(\det \left(\boldsymbol{M}_k + \frac{1}{\sigma_a^2 \tau} \boldsymbol{G}_{u,k} \tilde{S}_k \boldsymbol{G}_{u,k}^{\mathrm{H}} \right) \right) - \beta_k \mathrm{Tr}\left(\tilde{S}_k \right) \tag{28a}$$

$$\text{s.t. } \tilde{S}_k \succeq \boldsymbol{0} \tag{28b}$$

where $\boldsymbol{M}_k = \boldsymbol{I} + \boldsymbol{I}_{b,k}$. Define $\bar{\boldsymbol{G}}_{uk} = \boldsymbol{\Delta}_k^{-(1/2)} \boldsymbol{Q}_k^{\mathrm{H}} \boldsymbol{G}_{uk}$, where $\boldsymbol{\Delta}_k$ and $\boldsymbol{Q}_k$ are obtained via the eigenvalue decomposition of $\boldsymbol{M}_k$, i.e., $\boldsymbol{M}_k = \boldsymbol{Q}_k \boldsymbol{\Delta}_k \boldsymbol{Q}_k^{\mathrm{H}}$. Let $\bar{\boldsymbol{G}}_{uk} = \bar{\boldsymbol{U}}_k \bar{\boldsymbol{\Lambda}}_k \bar{\boldsymbol{V}}_k^{\mathrm{H}}$ as the singular value decomposition (SVD) of $\bar{\boldsymbol{G}}_{uk}$, where $\bar{\boldsymbol{\Lambda}}_k = $

diag$\{\bar{\lambda}_{k,1}, \ldots, \bar{\lambda}_{k,n}, \ldots, \bar{\lambda}_{k,N_k}\}$ with $\bar{\lambda}_{k,n}$ representing the nth singular value of $\bar{\boldsymbol{G}}_{uk}$. With these definitions, the optimal $\tilde{S}_k$ can be derived based on Proposition 2.

Proposition 2: The optimal solution to problem $\mathcal{P}6$ is $\tilde{S}_k = \bar{\boldsymbol{V}}_k \boldsymbol{P}_k \bar{\boldsymbol{V}}_k^{\mathrm{H}}$, where $\boldsymbol{P}_k = \mathrm{diag}\{p_{k,1}, \ldots, p_{k,n}, \ldots, p_{k,N_k}\}$ with $p_{k,n}$ obtained from the water-filling algorithm, i.e.,

$$p_{k,n} = \left[\frac{1}{\beta_k \ln 2} - \frac{\sigma_a^2 \tau}{\bar{\lambda}_{k,n}^2} \right]^+. \tag{29}$$

Proof: Refer to the Appendix. ∎

Then, for the optimization of τ with any given $\tilde{S}$ achieved by Proposition 2, let the first derivation of Lagrangian function (14) with respect to τ equal to zero, we have

$$\sum_{m=1}^{M} \ln\left(1 + \frac{\mu_m}{\sigma_a^2 \tau} \right) - \sum_{m=1}^{M} \frac{1}{1 + \frac{\sigma_a^2}{\mu_m} \tau} = \alpha P_a \ln 2 \tag{30}$$

where μ_m is the mth eigenvalue of matrix $\sum_{k=1}^{K} \boldsymbol{G}_{u,k} \tilde{S}_k \boldsymbol{G}_{u,k}^{\mathrm{H}}$. The optimal τ within $0 < \tau < 1$ can be obtained via solving (30). Denoting the left-hand side of (30) as $f(\tau)$, we can derive that

$$\frac{\mathrm{d}f(\tau)}{\mathrm{d}\tau} = - \sum_{m=1}^{M} \frac{\mu_m^2}{\sigma_a^4 \left(\tau + \frac{\mu_m}{\sigma_a^2} \right)^2} < 0. \tag{31}$$

Thus, $f(\tau)$ is a decreasing function and τ satisfying (30) can be uniquely determined by the bisection search.

Therefore, by iteratively updating $\tilde{S}$ and τ until the algorithm converges, all users' optimal uplink information covariance matrices with semi-closed forms and the optimal τ are obtained.

4) Fix {$\tilde{W}$, $\tilde{S}$, τ} and Optimize {α, $\boldsymbol{\beta}$, $\boldsymbol{\Psi}_w$, $\boldsymbol{\Psi}_s$}: The Lagrangian multipliers are updated by solving the Lagrangian dual problem, i.e., problem $\mathcal{P}5$. Since the objective function of problem $\mathcal{P}5$ is nondifferential, Lagrangian multipliers are updated by applying the subgradient method.

Specifically, the update of each β_k is expressed as

$$\beta_k := \beta_k - \delta_t \left(\rho_k \mathrm{Tr}\left(\boldsymbol{G}_{d,k}^{\mathrm{H}} \tilde{W} \boldsymbol{G}_{d,k} \right) - \mathrm{Tr}\left(\tilde{S}_k \right) \right) \tag{32}$$

where δ_t is the update step size. For the update of α, we revisit the proof of Proposition 1. In the proof, it has been demonstrated that $\alpha = \eta_{\max}$ is always satisfied at the optimum. Thus, the update of α is expressed as

$$\alpha = \eta\left(\sum_{k=1}^{K} \beta_k \rho_k \boldsymbol{G}_{d,k} \boldsymbol{G}_{d,k}^{\mathrm{H}} \right) \tag{33}$$

where function $\eta(\boldsymbol{A})$ is the maximum eigenvalue of matrix $\boldsymbol{A}$. Then, with the obtained $\boldsymbol{\beta}$ and α, the matrix multipliers $\boldsymbol{\Psi}_w$ and $\boldsymbol{\Psi}_s$ can be updated based on (20) and (25), respectively.

B. Downlink Passive Beamforming: Fix {$\boldsymbol{W}$, $\boldsymbol{S}$, τ} and Optimize $\boldsymbol{F}_d$

Notice that the objective function (11a) in problem $\mathcal{P}1$ is not related to $\boldsymbol{F}_d$, the optimization of $\boldsymbol{F}_d$ with any given $\boldsymbol{W}$ and $\boldsymbol{S}$ are reduced as the following feasibility check problem:

$$\mathcal{P}7 : \text{Find } \boldsymbol{F}_d \tag{34a}$$

$$\text{s.t. } f_{d,l} = \beta_l(\theta_{d,l})e^{j\theta_{d,l}}, \ \theta_{d,l} \in [-\pi, \pi) \ \forall l \tag{34b}$$

$$\tau \text{Tr}(\boldsymbol{S}_k) \leq (1-\tau)\rho_k \text{Tr}(\boldsymbol{G}_{d,k}^{\text{H}}\boldsymbol{W}\boldsymbol{G}_{d,k}) \ \forall k. \tag{34c}$$

To effectively deal with this problem, in what follows, we first transform problem $\mathcal{P}7$ into a tractable form and then propose a low-complexity algorithm.

1) Problem Transformation: To make the downlink passive beamforming $\boldsymbol{F}_d$ explicit in the expression of $\text{Tr}(\boldsymbol{G}_{d,k}^{\text{H}}\boldsymbol{W}\boldsymbol{G}_{d,k})$, we substitute $\boldsymbol{G}_{d,k}^{\text{H}} = \boldsymbol{H}_{a,k}^{\text{H}} + \boldsymbol{H}_{r,k}^{\text{H}}\boldsymbol{F}_d\boldsymbol{H}_{a,r}^{\text{H}}$ into $\text{Tr}(\boldsymbol{G}_{d,k}^{\text{H}}\boldsymbol{W}\boldsymbol{G}_{d,k})$ and then

$$\begin{aligned}\text{Tr}(\boldsymbol{G}_{d,k}^{\text{H}}\boldsymbol{W}\boldsymbol{G}_{d,k}) = &\text{Tr}(\boldsymbol{F}_d^{\text{H}}\boldsymbol{A}_{d,k}\boldsymbol{F}_d\boldsymbol{B}_d) + \text{Tr}(\boldsymbol{F}_d^{\text{H}}\boldsymbol{C}_{d,k}^{\text{H}}) \\ &+ \text{Tr}(\boldsymbol{F}_d\boldsymbol{C}_{d,k}) + \text{Tr}(\boldsymbol{H}_{a,k}^{\text{H}}\boldsymbol{W}\boldsymbol{H}_{a,k}) \end{aligned} \tag{35}$$

where $\boldsymbol{A}_{d,k} = \boldsymbol{H}_{r,k}\boldsymbol{H}_{r,k}^{\text{H}}$, $\boldsymbol{B}_d = \boldsymbol{H}_{a,r}^{\text{H}}\boldsymbol{W}\boldsymbol{H}_{a,r}$, and $\boldsymbol{C}_{d,k} = \boldsymbol{H}_{a,r}^{\text{H}}\boldsymbol{W}\boldsymbol{H}_{a,k}\boldsymbol{H}_{r,k}^{\text{H}}$. Due to the fact that $\boldsymbol{F}_d$ is a diagonal matrix, we have

$$\text{Tr}(\boldsymbol{F}_d^{\text{H}}\boldsymbol{A}_{d,k}\boldsymbol{F}_d\boldsymbol{B}_d) = \boldsymbol{f}_d^{\text{H}}(\boldsymbol{A}_{d,k} \odot \boldsymbol{B}_d^T)\boldsymbol{f}_d \text{ and} \tag{36}$$

$$\text{Tr}(\boldsymbol{F}_d\boldsymbol{C}_{d,k}) = \boldsymbol{c}_{d,k}^T\boldsymbol{f}_d \tag{37}$$

where $\boldsymbol{c}_{d,k} = \text{diag}(\boldsymbol{C}_{d,k})$. As a result, $\text{Tr}(\boldsymbol{G}_{d,k}^{\text{H}}\boldsymbol{W}\boldsymbol{G}_{d,k})$ can be expressed as

$$\text{Tr}(\boldsymbol{G}_{d,k}^{\text{H}}\boldsymbol{W}\boldsymbol{G}_{d,k}) = \boldsymbol{f}_d^{\text{H}}\boldsymbol{D}_{d,k}\boldsymbol{f}_d + 2\text{Re}\{\boldsymbol{f}_d^{\text{H}}\boldsymbol{c}_{d,k}^*\} + \text{Tr}(\boldsymbol{H}_{a,k}^{\text{H}}\boldsymbol{W}\boldsymbol{H}_{a,k}) \tag{38}$$

where $\boldsymbol{D}_{d,k} = \boldsymbol{A}_{d,k} \odot \boldsymbol{B}_d^T$. Since both $\boldsymbol{A}_{d,k}$ and $\boldsymbol{B}_d$ are nonnegative semi-definite matrices, $\boldsymbol{D}_{d,k}$ is a nonnegative semi-definite matrix.

With (38), the design of $\boldsymbol{F}_d$ is equivalently replaced by the optimization of $\boldsymbol{f}_d$. To find better $\boldsymbol{f}_d$, the feasibility check problem $\mathcal{P}7$ can be effectively tackled via a newly transformed optimization problem. By introducing additional variable $\boldsymbol{\phi} = [\phi_1, \ldots, \phi_K]^T$, the new tractable problem is formulated as

$$\mathcal{P}8 : \max_{\boldsymbol{f}_d, \boldsymbol{\theta}_d, \boldsymbol{\phi}} \sum_{k=1}^K \phi_k \tag{39a}$$

$$\text{s.t. } f_{d,l} = \beta_l(\theta_{d,l})e^{j\theta_{d,l}}, \ \theta_{d,l} \in [-\pi, \pi) \ \forall l \tag{39b}$$

$$\phi_k \geq 0 \ \forall k \tag{39c}$$

$$\phi_k + a_k \leq \boldsymbol{f}_d^{\text{H}}\boldsymbol{D}_{d,k}\boldsymbol{f}_d + 2\text{Re}\{\boldsymbol{f}_d^{\text{H}}\boldsymbol{c}_{d,k}^*\}\forall k \tag{39d}$$

where $a_k = (\tau/[\rho_k(1-\tau)])\text{Tr}(\boldsymbol{S}_k) - \text{Tr}(\boldsymbol{H}_{a,k}^{\text{H}}\boldsymbol{W}\boldsymbol{H}_{a,k})$.

2) Proposed Low-Complexity Algorithm: Problem $\mathcal{P}8$ is obvious nonconvex, owing to the nonconvex constraint (39b) and the nonconvex quadratic constraint (39d). To handle this problem with low computational complexity, in this article, we propose an SCA-based penalty function method consisting of two loops.

First, in the outer loop, the SCA method is adopted to deal with the nonconvex constraint (39d). In particular, the nonconvex part in (39d), $\boldsymbol{f}_d^{\text{H}}\boldsymbol{D}_{d,k}\boldsymbol{f}_d$, is iteratively replaced by its linear

form. As $\boldsymbol{f}_d^{\text{H}}\boldsymbol{D}_{d,k}\boldsymbol{f}_d$ is convex with respect to $\boldsymbol{f}_d$, we have

$$-\boldsymbol{f}_d^{(t)\text{H}}\boldsymbol{D}_{d,k}\boldsymbol{f}_d^{(t)} + 2\text{Re}\{\boldsymbol{f}_d^{\text{H}}\boldsymbol{D}_{d,k}\boldsymbol{f}_d^{(t)}\} \leq \boldsymbol{f}_d^{\text{H}}\boldsymbol{D}_{d,k}\boldsymbol{f}_d \tag{40}$$

where $\boldsymbol{f}_d^{(t)}$ is obtained from iteration t in the outer loop. Consequently, in iteration $t+1$, problem $\mathcal{P}8$ becomes

$$\mathcal{P}9: \max_{\boldsymbol{f}_d, \boldsymbol{\theta}_d, \boldsymbol{\phi}} \sum_{k=1}^K \phi_k \tag{41a}$$

$$\text{s.t. } f_{d,l} = \beta_l(\theta_{d,l})e^{j\theta_{d,l}} \tag{41b}$$

$$-\pi \leq \theta_{d,l} < \pi \ \forall l \tag{41c}$$

$$\phi_k \geq 0 \ \forall k \tag{41d}$$

$$\phi_k + b_k^{(t)} \leq \text{Re}\{\boldsymbol{f}_d^{\text{H}}\boldsymbol{d}_k^{(t)}\} \ \forall k \tag{41e}$$

where $b_k^{(t)} = (a_k + \boldsymbol{f}_d^{(t)\text{H}}\boldsymbol{D}_{d,k}\boldsymbol{f}_d^{(t)})/2$ and $\boldsymbol{d}_k^{(t)} = \boldsymbol{c}_{d,k}^* + \boldsymbol{D}_{d,k}\boldsymbol{f}_d^{(t)}$. Since the relaxation of (41e) is conservative, the obtained solution to problem $\mathcal{P}9$ is always feasible for problem $\mathcal{P}8$.

Then, in the inner loop, we propose an iterative algorithm based on the penalty function method to solve problem $\mathcal{P}9$, which adds the constraint-related penalty function in the objective and penalizes the violation of constraint via the penalty factor. In particular, by introducing the penalty factor $\mu \geq 0$ for (41b) and the penalty vector $\boldsymbol{v} = [v_1, \ldots, v_K]^T \succeq \boldsymbol{0}$ for (41e), the new objective function is expressed as

$$\begin{aligned}\sum_{k=1}^K \phi_k - \mu \sum_{l=1}^L &\left|\left[f_{d,l} - \beta_l(\theta_{d,l})e^{j\theta_{d,l}}\right]\right|^2 \\ &+ \sum_{k=1}^K v_k\left(\text{Re}\{\boldsymbol{f}_d^{\text{H}}\boldsymbol{d}_k^{(t)}\} - b_k^{(t)} - \phi_k\right). \end{aligned} \tag{42}$$

As a result, problem $\mathcal{P}9$ can be handled via the following problem:

$$\mathcal{P}10 : \max_{\boldsymbol{f}_d, \boldsymbol{\phi}, \boldsymbol{\theta}_d} \sum_{k=1}^K \phi_k(1 - v_k) + \text{Re}\left\{\boldsymbol{f}_d^{\text{H}}\left(\sum_{k=1}^K v_k\boldsymbol{d}_k^{(t)}\right)\right\}$$
$$-\mu \sum_{l=1}^L \left|f_{d,l} - \beta_l(\theta_{d,l})e^{j\theta_{d,l}}\right|^2 \tag{43a}$$

$$\text{s.t. } -\pi \leq \theta_{d,l} < \pi \ \forall l \tag{43b}$$

$$\phi_k \geq 0 \ \forall k \tag{43c}$$

where the objective function is obtained by rearranging (42).

It is observed that the optimization of $\{\boldsymbol{f}_d, \boldsymbol{\theta}_d\}$ and $\boldsymbol{\phi}$ is independent and can be solved in parallel. For the optimization of $\{\boldsymbol{f}_d, \boldsymbol{\theta}_d\}$, an iterative algorithm is proposed to alternatively update $\boldsymbol{f}_d$ and $\boldsymbol{\theta}_d$. With any given $\boldsymbol{f}_d = [\beta_l(\theta_{d,l})e^{j\theta_{d,l}}, \ldots, \beta_l(\theta_{d,L})e^{j\theta_{d,L}}]^T$, the $\boldsymbol{f}_d$-related optimization problem is simplified as

$$\mathcal{P}11 : \min_{\boldsymbol{f}_d} \ \mu\|\boldsymbol{f}_d - \bar{\boldsymbol{f}}_d\|^2 - \text{Re}\left\{\boldsymbol{f}_d^{\text{H}}\left(\sum_{k=1}^K v_k\boldsymbol{d}_k^{(t)}\right)\right\} \tag{44a}$$

whose optimal solution is $\boldsymbol{f}_d = \bar{\boldsymbol{f}}_d + (1/2\mu)(\sum_{k=1}^K v_k\boldsymbol{d}_k^{(t)})$. With any given $\boldsymbol{f}_d$, the $\boldsymbol{\theta}_d$-related optimization problem is expressed as

$$\mathcal{P}12 : \min_{\boldsymbol{\theta}_d} \ \mu \sum_{l=1}^{L} \left| f_{d,l} - \beta_l(\theta_{d,l}) e^{j\theta_{d,l}} \right|^2 \tag{45a}$$

$$\text{s.t.} \ -\pi \le \theta_{d,l} < \pi \ \forall l. \tag{45b}$$

Although problem $\mathcal{P}12$ is nonconvex, its element-wise optimal solution $\theta_{d,l}$ has been analytically derived in parallel in [28]. Furthermore, for the optimization of $\boldsymbol{\phi}$, problem $\mathcal{P}10$ is simplified as

$$\max_{\{\phi_k \ge 0\}} \sum_{k=1}^{K} \phi_k (1 - v_k). \tag{46}$$

To make sure that this problem has a finite objective value, the penalty factor should satisfy $v_k \ge 1$ and then the optimal ϕ_k is $\phi_k = 0 \ \forall k$. Thus, by alternatively optimization $\boldsymbol{f}_d$ and $\boldsymbol{\theta}_d$, problem $\mathcal{P}10$ can be solved.

In addition to the optimization of $\boldsymbol{f}_d$, $\boldsymbol{\theta}_d$, and $\boldsymbol{\phi}$, the penalty factors μ and $\boldsymbol{v}$ in problem $\mathcal{P}10$ also need to be updated accordingly. To penalize the violation of (41b), the value of μ should be enlarged with the increase of the number of iterations. Hence, the updated of μ is expressed as $\mu^{(i+1)} = \delta_{\mu,t}\mu^{(i)}$, where $\mu^{(i)}$ is the value of μ obtained from the ith iteration in the inner loop and $\delta_{\mu,t} > 0$ is the stepsize. For the update of $\boldsymbol{v}$, we can observe from problem $\mathcal{P}10$ that, if $\text{Re}\{\boldsymbol{f}_d^{\text{H}}\boldsymbol{d}_k^{(t)}\} < b_k^{(t)}$, v_k should be increased to penalize the violation of (41e). As a result, with any given $\boldsymbol{f}_d$, the penalty factor v_k is updated by

$$v_k^{(i+1)} = \left[v_k^{(i)} - \delta_t \left(\text{Re}\left\{ \boldsymbol{f}_d^{\text{H}} \boldsymbol{d}_k^{(t)} \right\} - b_k^{(t)} \right) \right]_1^+ \ \forall k \tag{47}$$

where $v_k^{(i)}$ is the value of v_k obtained from the ith iteration in the inner loop and $\delta_{v,t} > 0$ is the stepsize. Therefore, by iteratively updating $\{\boldsymbol{f}_d, \boldsymbol{\theta}_d\}$ and $\{\mu, \boldsymbol{v}\}$ in the inner loop, problem $\mathcal{P}9$ can be efficiently solved.

Finally, to summarize, the proposed SCA-based penalty function method consists of two loops. In the outer loop, the SCA method is adopted to conservatively linearize nonconvex part in (39d) and then problem $\mathcal{P}8$ is converted to problem $\mathcal{P}9$ in each iteration. In the inner loop, problem $\mathcal{P}9$ is solved via the penalty function method, which alternatively updates the optimization variables $\{\boldsymbol{f}_d, \boldsymbol{\theta}_d\}$ and the penalty factors $\{\mu, \boldsymbol{v}\}$. It is worth pointing out that both the analytical closed forms of $\boldsymbol{f}_d$ and $\boldsymbol{\theta}_d$ are derived in the inner loop. The detailed algorithm is outlined in Algorithm 2.

C. Uplink Passive Beamforming: Fix $\{\boldsymbol{W}, \boldsymbol{S}, \tau\}$ and Optimize $\boldsymbol{F}_u$

For the optimization of $\boldsymbol{F}_u$, the original problem $\mathcal{P}1$ with any given $\boldsymbol{W}$ and $\boldsymbol{S}$ is reduced as

$$\mathcal{P}13 : \max_{\boldsymbol{F}_u} \ \log_2\left(\det\left(\boldsymbol{I} + \frac{1}{\sigma_a^2} \sum_{k=1}^{K} \boldsymbol{G}_{u,k} \boldsymbol{S}_k \boldsymbol{G}_{u,k}^{\text{H}} \right) \right) \tag{48a}$$

$$\text{s.t.} \ f_{u,l} = \beta_l(\theta_{u,l}) e^{j\theta_{u,l}}, \ \theta_{u,l} \in [-\pi, \pi) \ \forall l. \tag{48b}$$

Denote $\boldsymbol{G}_u = [\boldsymbol{G}_{u,1}, \dots, \boldsymbol{G}_{u,K}]$ and $\hat{\boldsymbol{S}} = \text{diag}(\boldsymbol{S}_1, \dots, \boldsymbol{S}_K)$ as the aggregated channel matrix and the newly formed aggregated information covariance matrix, respectively. Problem

---

Algorithm 2 Downlink Passive Beamforming Design to Maximize the Uplink Sum Rate

1: Set $t = 0$ and initialize $\boldsymbol{f}_d^{(0)}$;
2: **while** The stopping criteria of the outer loop is not satisfied **do**
3:    Calculate $b_k^{(t)} = (a_k + \boldsymbol{f}_d^{(t)H}\boldsymbol{D}_{d,k}\boldsymbol{f}_d^{(t)})/2$ and $\boldsymbol{d}_k^{(t)} = \boldsymbol{c}_{d,k}^* + \boldsymbol{D}_{d,k}\boldsymbol{f}_d^{(t)}$;
4:    Set $i = 0$ and initialize penalty factors $\mu^{(0)}$ and $\boldsymbol{v}_k^{(0)}$;
5:    **while** The stopping criteria of the inner loop is not satisfied **do**
6:       Update $\boldsymbol{f}_d = \bar{\boldsymbol{f}}_d + \frac{1}{2\mu}(\sum_{k=1}^{K} v_k \boldsymbol{d}_k^{(t)})$;
7:       Update $\boldsymbol{\theta}_d$ according to [28];
8:       Update $\mu^{(i+1)} = \delta_{\mu,t}\mu^{(i)}$;
9:       Update $v_k^{(i+1)} = \left[v_k^{(i)} - \delta_t \left(\text{Re}\{\boldsymbol{f}_d^{(i)H}\boldsymbol{d}_k^{(t)}\} - b_k^{(t)} \right) \right]_1^+$;
10:       Set $i = i + 1$;
11:    **end while**
12:    $\boldsymbol{f}_d^{(t)} = \boldsymbol{f}_d^{(i)}$;
13:    Set $t = t + 1$;
14: **end while**
15: **return** $\boldsymbol{f}_d$.

$\mathcal{P}13$ can be equivalently reformulated as

$$\mathcal{P}14 : \max_{\boldsymbol{F}_u} \ \tau \log_2\left(\det\left(\boldsymbol{I} + \frac{1}{\sigma_a^2} \boldsymbol{G}_u \hat{\boldsymbol{S}} \boldsymbol{G}_u^{\text{H}} \right) \right) \tag{49a}$$

$$\text{s.t.} \ f_{u,l} = \beta_l(\theta_{u,l}) e^{j\theta_{u,l}}, \ \theta_{u,l} \in [-\pi, \pi) \ \forall l \tag{49b}$$

where $\boldsymbol{G}_u = \boldsymbol{H}_a + \boldsymbol{H}_{a,r}\boldsymbol{F}_u\boldsymbol{H}_r$ with $\boldsymbol{H}_a = [\boldsymbol{H}_{a,1}, \dots, \boldsymbol{H}_{a,K}]$ and $\boldsymbol{H}_r = [\boldsymbol{H}_{r,1}, \dots, \boldsymbol{H}_{r,K}]$. By aggregating the channel matrices and information covariance matrices of multiple users, problem $\mathcal{P}14$ has the same form as the single-user rate maximization problem and can be regarded as a virtual single-user problem. The key of this problem is how to configure the uplink channel matrix $\boldsymbol{G}_u$ (i.e., $\boldsymbol{F}_u$) to maximize the single-user channel capacity.

Notice that the objective function (49a) is complicated with respect to $\boldsymbol{F}_u$, it is impossible to directly solve problem $\mathcal{P}14$. To tackle this obstacle, we resort to the method proposed in [13] and [37], with which (49a) is first equivalently rewritten as a function of passive reflecting element $f_{u,l}$ and then each $f_{u,l}$ is iteratively updated with the satisfaction of (49b) until the algorithm converges. The detailed algorithm refers to [13, Algorithm 1] and [37].

D. Overall Algorithm

To sum up, the formulated uplink sum-rate maximization problem $\mathcal{P}1$ is handled via alternatively optimizing variable blocks $\{\boldsymbol{W}, \boldsymbol{S}, \tau\}$, $\boldsymbol{F}_d$ and $\boldsymbol{F}_u$, where $\boldsymbol{F}_d$ and $\boldsymbol{F}_u$ are optimized in parallel. With any given channel configuration matrices $\boldsymbol{F}_d$ and $\boldsymbol{F}_u$, the globally optimal $\boldsymbol{W}$, $\boldsymbol{S}$, and τ are achieved by the proposed algorithm (Algorithm 1), due to the fact that problem $\mathcal{P}3$ is convex and can be optimally handled via the Lagrangian method. More importantly, the optimal rank-one $\tilde{\boldsymbol{W}}$ is derived, and the optimal semi-closed $\tilde{\boldsymbol{S}}$ is obtained. With the given

Algorithm 3 Proposed Joint Active and Passive Beamforming Framework

1: Initialize $\boldsymbol{F}_d$ and $\boldsymbol{F}_u$;
2: **while** the stopping criteria is not satisfied **do**
3:     Update $\boldsymbol{W}$, $\boldsymbol{S}$ and τ via the proposed **Algorithm 1**;
4:     Update $\boldsymbol{F}_d$ and $\boldsymbol{F}_u$ via the proposed **Algorithm 2** and Algorithm 1 in [37], respectively;
5: **end while**
6: Update $\boldsymbol{S}_k = \frac{\max(\mathrm{trace}(\boldsymbol{S}_k), P_{k,\mathrm{sensitivity}})}{\mathrm{trace}(\boldsymbol{S}_k)} \boldsymbol{S}_k, \forall k$;
7: **return** $\boldsymbol{W}$, $\boldsymbol{S}$, τ, $\boldsymbol{F}_d$ and $\boldsymbol{F}_u$.

Fig. 2. Projected horizontal network topology of the simulation scenario.

$\{\boldsymbol{W}, \boldsymbol{S}, \tau\}$, $\boldsymbol{F}_d$ and $\boldsymbol{F}_u$ are, respectively, and concurrently optimized via the proposed algorithm (Algorithm 2) and [13, Algorithm 1]. Since problems $\mathcal{P}8$ and $\mathcal{P}13$ are nonconvex and solved via the alternative optimization method, the achieved $\boldsymbol{F}_d$ and $\boldsymbol{F}_u$ are locally optimal. Repeat these two procedures until the value of the objective function converges, problem $\mathcal{P}1$ can be solved. The framework of the proposed joint active and passive beamforming design is summarized in Algorithm 3, where the operation in line 6 is to make sure that the EH circuit only works when the received power is larger than the EH sensitivity power point $P_{k,\mathrm{sensitivity}}$. The output of Algorithm 3 is obvious a local optimal solution to problem $\mathcal{P}1$, as $\{\boldsymbol{W}, \boldsymbol{S}, \tau\}$, $\boldsymbol{F}_d$ and $\boldsymbol{F}_u$ are alternatively optimized.

To analyze the time complexity of the overall Algorithm 3, we first show the complexity of algorithms for subproblems. For the optimization of $\{\boldsymbol{W}, \boldsymbol{S}, \tau\}$ with Algorithm 1, let $N_{1,\mathrm{outer}}$ and $N_{1,\mathrm{inner}}$, respectively, denote the number of iterations in the outer loop and the inner loop. The time complexity is $\mathcal{O}_1 = \mathcal{O}(N_{1,\mathrm{outer}}(N_{1,\mathrm{inner}}(\sum_{k=1}^K (MN_k^2 + N_k^3 + \log_2(1/\epsilon_\tau))) + M^3))$, where ϵ_τ is the error threshold when solving τ with the bisection method. For the optimization of $\boldsymbol{F}_d$ with Algorithm 2, denote by $N_{2,\mathrm{outer}}$ and $N_{2,\mathrm{inner}}$, respectively, the number of iterations in the outer loop and the inner loop. The complexity is $\mathcal{O}_2 = \mathcal{O}(N_{2,\mathrm{outer}}(N_{2,\mathrm{inner}}L + K))$. For the optimization of $\boldsymbol{F}_u$ with [37, Algorithm 1], the complexity is $\mathcal{O}_3 = \mathcal{O}(((3M^3 + 2M^2(\sum_{k=1}^K N_k) + (\sum_{k=1}^K N_k)^2)L + M(\sum_{k=1}^K N_k)\min(M, \sum_{k=1}^K N_k))N_{3,\mathrm{ite}})$, where $N_{3,\mathrm{ite}}$ is the number of iterations in [37, Algorithm 1]. Therefore, the time complexity of Algorithm 3 is $\mathcal{O}((\mathcal{O}_1 + \mathcal{O}_2 + \mathcal{O}_3)N_{\mathrm{all}})$, where N_{all} is the number of iterations in Algorithm 3.

For the practical implementation, the proposed algorithm must be operated within the channel coherence time. In our considered IRS-assisted WPCNs, all nodes, including the AP, the IRS, and IoT users, are deployed in fixed positions without any movement. Hence, the channel coherence time of the considered quasi-static scenario is longer than that defined by 3GPP and may fall into tens of milliseconds. Within this relatively long channel coherence time, our proposed algorithm is also designed with partial parallel processing, which significantly reduces the computing time. In specific, the downlink passive beamforming $\boldsymbol{F}_d$ and the uplink passive beamforming $\boldsymbol{F}_u$ are designed in parallel with any given active beamforming $\{\boldsymbol{W}, \boldsymbol{S}, \tau\}$. Within the optimization of active beamforming $\{\boldsymbol{W}, \boldsymbol{S}, \tau\}$, $\boldsymbol{W}$ and $\{\boldsymbol{S}, \tau\}$ are designed in parallel. Within the optimization of downlink passive beamforming $\boldsymbol{F}_d$, each
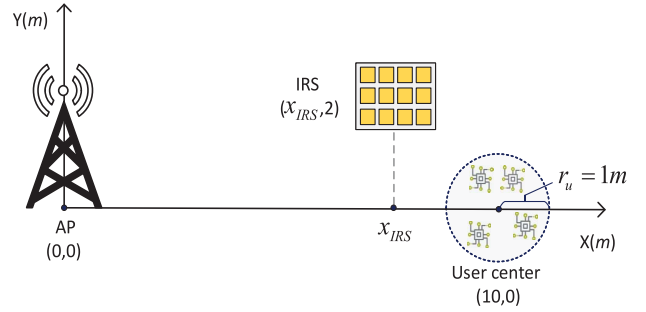
element of IRS $f_{d,l}$ is also derived in parallel. Furthermore, in practical communication systems, the proposed joint active and passive beamforming algorithm belongs to the physical layer signal processing and is running on the FPGA, which is natural for the parallel computing. With enough FPGA resource, carefully designed parallel computing and specific hardware acceleration, it is possible to estimate the CSI and obtain the proposed solution in a relatively long channel coherence time.

IV. NUMERICAL RESULTS

In this section, extensive numerical simulations are conducted to validate the effectiveness of our proposed algorithm in the considered IRS-aided WPCN.

A. Simulation Setup

Throughout the simulations, we consider a 3-D IRS-assisted scenario, whose projected horizontal network topology is shown in Fig. 2. In the scenario, one AP serves $K = 4$ energy-constrained IoT users and one IRS is deployed near the IoT users to construct extra reflection links. In specific, under a 3-D Cartesian coordinate system, the AP is located at (0 m, 0 m, 2 m) and the IRS is located at (x_{IRS}, 2 m, 2 m), where x_{IRS} is the horizontal axis of the IRS with $x_{\mathrm{IRS}} = 8$ m unless otherwise specified. IoT users are uniformly distributed within a circle of radius $r_u = 1$ m and the circle center is set as (10 m, 0 m, 0 m). In the setup, the AP has $M = 8$ antennas and each IoT user has $N_k = 2$ antennas. The IRS is equipped with a uniform planar array with $L = L_x L_y$ reflecting elements, where $L_x = 10$ and L_y are, respectively, denote the number of reflecting elements in horizontal and vertical directions. In addition, the transmission power of AP is set as $P_a = 25$ dBm and the noise power is set as $\sigma_a^2 = -104$ dBm. As the received RF energy at each IoT user cannot be entirely converted to the available energy, the EH efficiency is set as $\rho_k = 0.5$. The parameters related to the practical phase shift model are, respectively, set as $\beta_{\min} = 0.2$, $\bar{\theta} = 0.43\pi$, and $\chi = 1.6$ in accordance with [28].

The wireless channel model is composed of the large-scale path loss model and the small-scale fading model. The large-scale path-loss model is dependent on the communication distance between the transmitter and the receiver. Let d be

the communication distance, the path-loss model is given as

$$\mathrm{PL}(d) = C_0 \left(\frac{d}{d_0} \right)^{-\kappa} \tag{50}$$

where $C_0 = -30$ dB is the large-scale path loss at the reference distance $d_0 = 1$ m and κ is the path-loss exponent. In this simulation, the path-loss exponents for the AP–user link, the AP–IRS link, and the IRS–user link are, respectively, set as $\kappa_{a,u} = 3.5$, $\kappa_{a,r} = 2.2$, and $\kappa_{r,u} = 2.8$. For the small-scale channel fading, Rician fading is adopted here. Mathematically, the small-scale channel model is expressed as

$$\boldsymbol{H} = \sqrt{\frac{\omega}{1+\omega}} \boldsymbol{H}^{\mathrm{LoS}} + \sqrt{\frac{1}{1+\omega}} \boldsymbol{H}^{\mathrm{NLoS}} \tag{51}$$

where $\boldsymbol{H} \in \{\boldsymbol{H}_{a,k}, \boldsymbol{H}_{a,r}, \boldsymbol{H}_{r,k}\}$, $\boldsymbol{H}^{\mathrm{LoS}}$ and $\boldsymbol{H}^{\mathrm{NLoS}}$ are, respectively, denote the Line-of-Sight (LoS) and non-LoS (NLoS) components of channel $\boldsymbol{H}$, and $\omega \in [0, \infty)$ represents the Rician factor. In (51), $\boldsymbol{H}^{\mathrm{LoS}}$ is constructed by the product of array steering vectors at both the receiver and the transmitter, i.e., $\boldsymbol{H}^{\mathrm{LoS}} = \boldsymbol{a}_R(\phi_A, \psi_A)\boldsymbol{a}_T(\phi_D, \psi_D)^{\mathrm{H}}$, where $\phi_A(\phi_D)$ and $\psi_A(\phi_D)$ are, respectively, the azimuth and elevation angles of arrival (departure). Specific expressions of $\boldsymbol{a}_R(\phi_A, \psi_A)$ and $\boldsymbol{a}_T(\phi_D, \psi_D)$ are related to their corresponding array types, i.e., ULA or UPA, and can be found in [13]. In the simulation, $\phi_A(\phi_D)$ and $\psi_A(\phi_D)$ are uniformly chosen from $[0, 2\pi)$ and $[0, \pi)$, respectively. Then, for the NLoS channel model in (51), $\boldsymbol{H}^{\mathrm{NLoS}}$ is characterized by Rayleigh fading with each element following $\mathcal{CN}(0, 1)$. Notice that the Rician factor ω is in fact a weighting factor between the LoS and NLoS channel components. When $\omega = 0$, $\boldsymbol{H}$ is totally a NLoS Rayleigh channel; while when $\omega \to \infty$, $\boldsymbol{H}$ approaches to a deterministic LoS channel. Denote by $\omega_{a,u}$, $\omega_{a,r}$, and $\omega_{r,u}$, respectively, the Rician factors of the AP–user link, the AP–IRS link, and the IRS–user link. In the simulation, We set $\omega_{a,u} = 0$, $\omega_{a,r} = 1$, and $\omega_{r,u} = 0$.

B. Baseline Algorithms

To comprehensively appraise the performance of our proposed algorithm, labeled as "proposed algorithm," four baseline algorithms are also conducted in the simulation. These baseline algorithms are classified as three categories: 1) the simplified passive beamforming algorithms (baselines 1 and 3); 2) the simplified active beamforming algorithm (baseline 2); and 3) the baseline algorithm without the deployment of IRS (baseline 4). The detailed baseline algorithms are shown in the following, whose time complexity analysis is listed in Table I.

1) *Uplink Channel Gain Max:* In this algorithm, the uplink channel configuration matrix $\boldsymbol{F}_u$ is optimized via the channel power gain maximization algorithm. Then, $\{\boldsymbol{W}, \boldsymbol{S}, \tau\}$ and $\boldsymbol{F}_d$ are alternatively optimized via Algorithms 1 and 2.

2) *Simplified $\boldsymbol{S}$ Optimization*: In this algorithm, the uplink information covariance $\boldsymbol{S}_k$ in Algorithm 1 is designed via the SVD of channel $\boldsymbol{G}_{u,k}$, ignoring the interuser interference. Then, other variables are optimized in the same way as Algorithm 3.

TABLE I
TIME COMPLEXITY ANALYSIS OF BASELINE ALGORITHMS

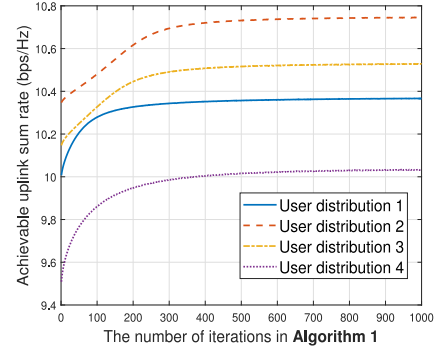| Baseline Algorithms	Time Complexity
Uplink channel gain max.	$\mathcal{O}_3 + \mathcal{O}((\mathcal{O}_1 + \mathcal{O}_2)N_{\mathrm{all}})$
Simplified $\boldsymbol{S}$ optimization	$\mathcal{O}\Big(\big(((\log_2 \frac{1}{\epsilon_\tau} + M^3)N_{1,\mathrm{outer}} + \sum_{k=1}^{K}(MN_k^2)) + \mathcal{O}_2 + \mathcal{O}_3 \big)N_{\mathrm{all}} \Big)$
Random phase shift	$\mathcal{O}(2L) + \mathcal{O}_1$
Without IRS	$\mathcal{O}_1$

Fig. 3. Convergence behavior of the active beamforming design.

3) *Random Phase Shift*: All phase shifts of IRS elements in both the downlink and uplink are randomly chosen from $[0, 2\pi]$. Then, the active beamforming matrix block $\{\boldsymbol{W}, \boldsymbol{S}, \tau\}$ is optimized via Algorithm 1.

4) *Without IRS*: In this scheme, the achievable uplink sum rate is maximized with the conventional system setup, where the IRS is not deployed. Hence, in the algorithm, the active beamforming matrix block $\{\boldsymbol{W}, \boldsymbol{S}, \tau\}$ is optimized via Algorithm 1 with $\boldsymbol{F}_u = \boldsymbol{F}_d = \boldsymbol{0}$.

C. Convergence Performance of Proposed Algorithms

In this section, the convergence performance of all proposed algorithms is investigated. With four independent user distributions and channel realizations, the convergence behaviors of proposed algorithms for solving the original problem $\mathcal{P}1$ are presented. First, in Fig. 3, the proposed algorithm (Algorithm 1) to design the active beamforming matrices can converge to the optimal point within 400 iterations. Since the analytical active beamforming matrices presented in Propositions 1 and 2 are derived in each iteration, the consumed time for the convergence of the algorithm is significantly reduced compared with the general CVX toolbox. Then, in Fig. 4, we can see that the proposed algorithm (Algorithm 2) to obtain the downlink passive beamforming matrix can converge within five iterations. Finally, the convergence behavior of the proposed joint active and passive beamforming algorithm, i.e., Algorithm 3, is shown in Fig. 5. For all four independent user distributions and channel realizations, the proposed algorithm can converge in about ten iterations. In the following sections, all results are averaged over 100 independent user distributions and channel realizations to make the results reliable and the curve smooth.
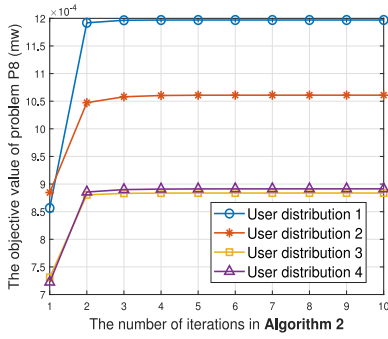
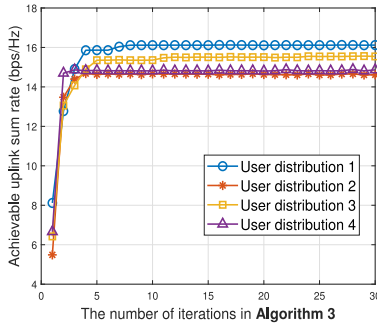Fig. 4. Convergence behavior of the downlink passive beamforming design.

Fig. 5. Convergence behavior of the proposed joint active and passive beamforming design.

D. Comparison Between Practical and Ideal Phase Shift Models

In this section, we compare the performance of the achievable uplink sum rate between our considered practical phase shift model and the ideal phase shift model. In the ideal model, the reflecting amplitude of each IRS element is assumed to be 1 and only the phase shift is flexibly adjusted. In Fig. 6, the solid and dashed curves are, respectively, the practical and ideal phase shift models in different algorithms with the varying of the number of IRS elements. As expected, by ignoring the relationship between the reflecting amplitude and the phase shift, the performance of the ideal phase shift model serves an upper bound of the practical phase model. Second, with the increase of the number of IRS elements, the uplink sum rates of conducted IRS-related algorithms are all growing. This is because more number of IRS elements provides much more room for the wireless channel configuration, which can better reflect the signal to the desired direction. Third, it is worth pointing out that, the proposed algorithm always outperforms other algorithms with the same phase shift model, and the performance gap gradually becomes wide with the increase of the number of IRS elements. In particular, when the number of IRS elements is 100, our proposed algorithm with the practical phase shift model can enlarge the uplink sum rate up to 50% compared with the scheme without IRS. Fourth, the performance of the simplified S optimization is even worse than the scheme without IRS when the number of IRS elements is lower than 40, and the situation is improved with the increase of the number of IRS elements. This may because the benefit brought by the wireless channel configuration
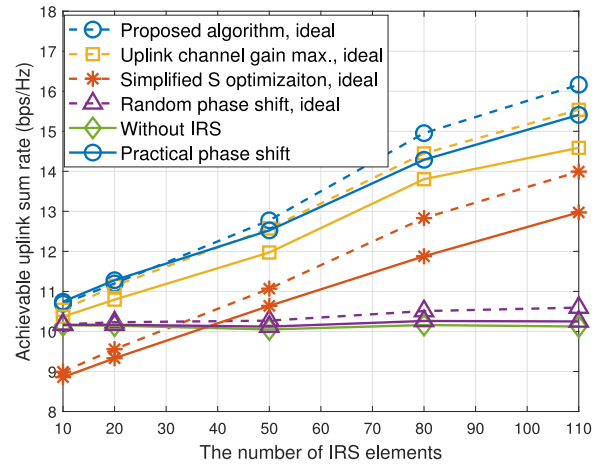

Fig. 6. Achievable uplink sum rate versus the number of IRS elements with practical and ideal phase shift model.
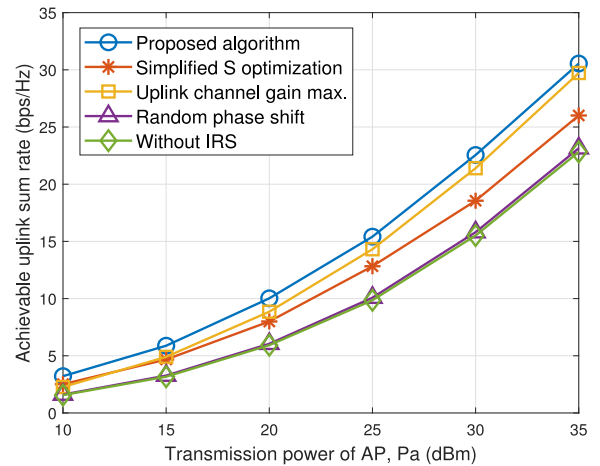

Fig. 7. Achievable uplink sum rate versus the transmission power of AP.

gradually makes up the performance deterioration resulted by the interuser interference.

E. Impact of Key System Parameters on the Achievable Uplink Sum Rate

The effect of key system parameters on the achievable uplink sum rate with the practical phase shift model is shown in this section. In Fig. 7, we plot the achievable uplink sum rates for all algorithms with the transmission power of AP sweeping from 10 to 35 dBm. It can be seen that the achievable uplink sum rate is improving with the increase of the transmission power. More importantly, the proposed joint active and passive beamforming design algorithm always has superior rate performance than other algorithms.

Fig. 8 shows the achievable uplink sum rate versus the number of IoT users for all algorithms. As expected, we can see that more number of IoT users leads to a higher achievable uplink sum rate. Furthermore, the appropriate wireless channel configuration can bring huge advantage compared with the random phase shift scheme and the scheme without IRS, and our proposed algorithm always outperforms other algorithms.

The impact of the number of antennas equipped by each IoT user on the achievable uplink sum rate is plotted in Fig. 9.
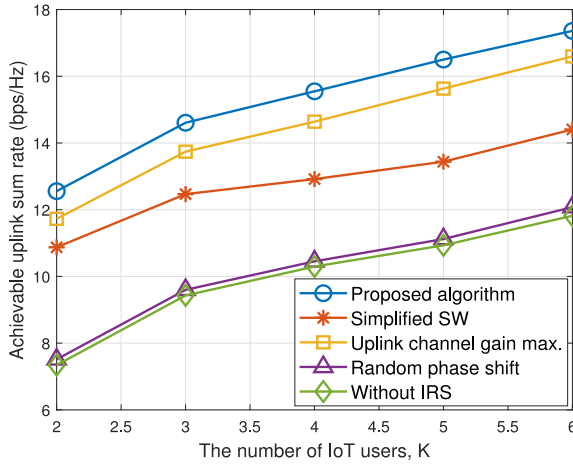
Fig. 8. Achievable uplink sum rate versus the number of users with $P_a = 25$ dBm.
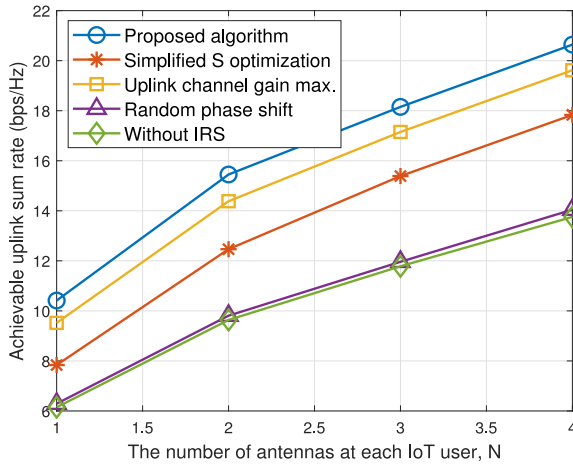

Fig. 10. Achievable uplink sum rate versus the location of the IRS with $P_a = 25$ dBm.

Fig. 9. Achievable uplink sum rate versus the number of antennas at IoT users with $P_a = 25$ dBm.

Fig. 11. Achievable uplink sum rate versus the number of IRS elements for different CE errors with $P_a = 25$ dBm.

With the increase of the number of antennas, the performance of all algorithms is improved, due to the spatial resource brought by more antennas. Furthermore, our proposed algorithm significantly outperforms other algorithms, especially the scheme without IRS, and the performance gap becomes wider with more antennas at IoT users.

In Fig. 10, the impact of IRS's location on the achievable uplink sum rate is shown for all algorithms. In the simulation, the horizontal axis of the IRS is changed from 1 to 9 m and other settings remain the same. As expected, with the movement of IRS, appropriate wireless channel configuration can always greatly enlarge the achievable uplink sum rate, and our proposed algorithm always outperforms other algorithms. Furthermore, when IRS moves from AP to users, the achievable uplink sum rates of the proposed algorithm and baseline algorithms 1–3 first decrease and then increase. The best rate performance is achieved when IRS is deployed closely near to users. The reason of this observed phenomena can be given as follows. Since AP is equipped with more number of antennas than each IoT user, the system performance is limited to IRS–user links compared with the AP–IRS link. When IRS is closer to AP, the channel quality of the AP–IRS link is good enough to compensate the weak IRS–user links and thus the
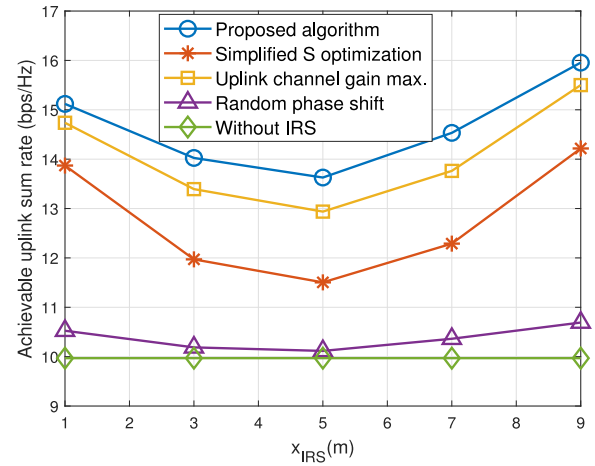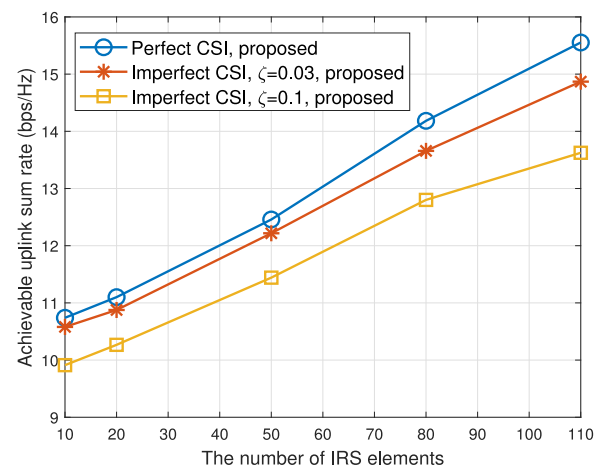
sum rate is enlarged at a certain degree. When IRS is closer to IoT users, the channel quality of both the IRS–user and AP–IRS links is strong, resulting in a higher sum rate. This observation provides a significant guideline for the practical deployment of IRS.

F. Impact of Imperfect CSI on the Achievable Uplink Sum Rate

In this section, we evaluate the impact of imperfect CSI on the system performance. The real channel model is expressed as

$$H = \bar{H} + \Delta H \qquad (52)$$

where $\bar{H}$ and ΔH are, respectively, the estimated CSI and the corresponding estimation error. Denote by $\zeta = \|\Delta H\|_F / \|\bar{H}\|_F$ the relative amount of CSI uncertainty.

Fig. 11 plots the achievable uplink sum rate versus the number of IRS elements with different channel uncertainty. For the imperfect CSI case, the joint active and passive beamforming is first optimized by our proposed algorithm based on the estimated CSI. Then, the designed beamforming is applied in the real channel to obtain the achievable uplink sum rate. As

expected, the CE error results in the system performance loss. Furthermore, with the increase of the number of IRS elements, the channel mismatch becomes severe and the performance gap between the perfect and imperfect CSI gradually broaden.

V. Conclusion

In this article, we have investigated an IRS-aided WPCN with a multiuser MIMO setup and the practical phase shift model, where the harvest-then-transmit protocol is adopted. To maximize the uplink sum rate, AP and IoT users' active beamforming, IRS's passive beamforming in the downlink and uplink, and the time allocation ratio have been jointly designed. These optimization variables have been divided into three blocks, i.e., the active beamforming, the downlink passive beamforming, and the uplink passive beamforming, and alternatively optimized. Numerical results have shown that the IRS with proper wireless channel configurations can significantly enlarge the uplink sum rate compared with the random phase shift scheme and the conventional scheme without IRS. To a certain degree, the performance gain is achieved on the basis of the CE of IRS-related links. More accurate CE usually consumes more pilot resources. In the future, we will jointly investigate the CE method and the active and passive beamforming design with practical phase shift to characterize a better tradeoff between the pilot resource cost and the network performance gain.

Appendix

As M_k is a symmetric positive-definite matrix, its eigenvalue decomposition is given as $M_k = Q_k \Delta_k Q_k^H$, where Q_k is a unitary matrix and Δ_k is a diagonal matrix. Define $\bar{G}_{uk} = \Delta_k^{-(1/2)} Q_k^H G_{uk}$, we have

$$
\begin{aligned}
&\log_2\left(\det\left(M_k + \frac{1}{\sigma_a^2 \tau} G_{u,k} \tilde{S}_k G_{u,k}^H\right)\right) \\
&= \log_2\left(\det\left(I + \frac{1}{\sigma_a^2 \tau} \bar{G}_{u,k} \tilde{S}_k \bar{G}_{u,k}^H\right)\right) + \log_2(\det(M_k)).
\end{aligned}
\tag{53}
$$

Decompose $\bar{G}_{uk} = \bar{U}_k \bar{\Lambda}_k \bar{V}_k^H$ via SVD and define $P_k = \bar{V}_k^H \tilde{S}_k \bar{V}_k$. Since $\text{Tr}(P_k) = \text{Tr}(\tilde{S}_k)$, problem $\mathcal{P}6$ is equivalently recast as

$$
\max_{P_k} \ \log_2\left(\det\left(I + \frac{1}{\sigma_a^2 \tau} \bar{\Lambda}_k P_k \bar{\Lambda}_k^H\right)\right) - \beta_k \text{Tr}(P_k) \tag{54a}
$$
$$
\text{s.t. } P_k \succeq \mathbf{0}. \tag{54b}
$$

By applying Hadamard's inequality [38], we have

$$
\det\left(I + \frac{1}{\sigma_a^2 \tau} \bar{\Lambda}_k P_k \bar{\Lambda}_k^H\right) \le \prod_{n=1}^{N_k}\left(1 + \frac{\bar{\lambda}_{k,n}^2 p_{k,n}}{\sigma_a^2 \tau}\right) \tag{55}
$$

where $\bar{\lambda}_{k,n}$ is nth diagonal element of $\bar{\Lambda}_k$. The equality holds when $\bar{\Lambda}_k P_k \bar{\Lambda}_k^H$ is diagonal, which means the optimal P_k is diagonal, i.e., $P_k = \text{diag}\{p_{k,1}, \ldots, p_{k,n}, \ldots, p_{k,N_k}\}$.

Then, with the diagonal P_k, problem (54) is reformulated as

$$
\max_{P_k} \ \sum_{n=1}^{N_k} \log_2\left(1 + \frac{1}{\sigma_a^2 \tau} \bar{\lambda}_{k,n}^2 p_{k,n}\right) - \sum_{n=1}^{N_k} \beta_k p_{k,n} \tag{56a}
$$

$$
\text{s.t. } p_{k,n} \ge 0 \ \forall n \tag{56b}
$$

whose optimal solution is $p_{k,n} = [(1/\beta_k \ln 2) - (\sigma_a^2 \tau / \bar{\lambda}_{k,n}^2)]^+$, obtained via the water-filling algorithm. Therefore, we have $\tilde{S}_k = \bar{V}_k P_k \bar{V}_k^H$. This completes the proof.

References

[1] A. Passarella and M. Conti, "Cisco annual Internet report (2018-2023)," San Francisco, CA, USA, White Paper, Mar. 2020. [Online]. Available: https://www.cisco.com/c/en/us/solutions/collateral/executive-perspectives/Annu.-internet-Rep./white-paper-c11-741490.html

[2] R. Zhang and C. K. Ho, "MIMO broadcasting for simultaneous wireless information and power transfer," *IEEE Trans. Wireless Commun.*, vol. 12, no. 5, pp. 1989–2001, May 2013.

[3] Q. Shi, L. Liu, W. Xu, and R. Zhang, "Joint transmit beamforming and receive power splitting for MISO SWIPT systems," *IEEE Trans. Wireless Commun.*, vol. 13, no. 6, pp. 3269–3280, Jun. 2014.

[4] Y. Wang, R. Sun, and X. Wang, "Transceiver design to maximize the weighted sum secrecy rate in full-duplex SWIPT systems," *IEEE Signal Process. Lett.*, vol. 23, no. 6, pp. 883–887, Jun. 2016.

[5] S. Bi, Y. Zeng, and R. Zhang, "Wireless powered communication networks: An overview," *IEEE Wireless Commun.*, vol. 23, no. 2, pp. 10–18, Apr. 2016.

[6] R. Sun, Y. Wang, R. Su, N. Cheng, and X. Shen, "A destination-aided wireless energy transfer scheme in multi-antenna relay sensor networks," *IEEE Wireless Commun. Lett.*, vol. 8, no. 3, pp. 689–692, Jun. 2019.

[7] X. Liu, Z. Qin, Y. Gao, and J. A. McCann, "Resource allocation in wireless powered IoT networks," *IEEE Internet Things J.*, vol. 6, no. 3, pp. 4935–4945, Jun. 2019.

[8] T. Xiaomi. "Forget about cables and charging stands with revolutionary MI air charge technology." Jan. 2021. [Online]. Available: https://blog.mi.com/en/2021/01/29/forget-about-cables–charging-stands–revolutionary-mi-air-charge-Technol./

[9] Z. Yin et al., "UAV-assisted physical layer security in multi-beam satellite-enabled vehicle communications," *IEEE Trans. Intell. Transp.*, vol. 23, no. 3, pp. 2739–2751, Mar. 2022.

[10] Y.-C. Liang, R. Long, Q. Zhang, J. Chen, H. V. Cheng, and H. Guo, "Large intelligent surface/antennas (LISA): Making reflective radios smart," *J. Commun. Inf. Netw.*, vol. 4, no. 2, pp. 40–50, Jun. 2019.

[11] E. Basar, M. D. Renzo, J. De Rosny, M. Debbah, M.-S. Alouini, and R. Zhang, "Wireless communications through reconfigurable intelligent surfaces," *IEEE Access*, vol. 7, pp. 116753–116773, 2019.

[12] S. Gong et al., "Toward smart wireless communications via intelligent reflecting surfaces: A contemporary survey," *IEEE Commun. Surveys Tuts.*, vol. 22, no. 4, pp. 2283–2314, 4th Quart., 2020.

[13] S. Zhang and R. Zhang, "Capacity characterization for intelligent reflecting surface aided MIMO communication," *IEEE J. Sel. Areas Commun.*, vol. 38, no. 8, pp. 1823–1838, Aug. 2020.

[14] C. Pan et al., "Multicell MIMO communications relying on intelligent reflecting surfaces," *IEEE Trans. Wireless Commun.*, vol. 19, no. 8, pp. 5218–5233, Aug. 2020.

[15] Q. Wu and R. Zhang, "Weighted sum power maximization for intelligent reflecting surface aided SWIPT," *IEEE Wireless Commun. Lett.*, vol. 9, no. 5, pp. 586–590, May 2020.

[16] C. Pan et al., "Intelligent reflecting surface aided MIMO broadcasting for simultaneous wireless information and power transfer," *IEEE J. Sel. Areas Commun.*, vol. 38, no. 8, pp. 1719–1734, Aug. 2020.

[17] Q. Wu and R. Zhang, "Joint active and passive beamforming optimization for intelligent reflecting surface assisted SWIPT under QoS constraints," *IEEE J. Sel. Areas Commun.*, vol. 38, no. 8, pp. 1735–1748, Aug. 2020.

[18] S. Zargari, A. Khalili, Q. Wu, M. R. Mili, and D. W. K. Ng, "Max-min fair energy-efficient beamforming design for intelligent reflecting surface-aided SWIPT systems with non-linear energy harvesting model," *IEEE Trans. Veh. Technol.*, vol. 70, no. 6, pp. 5848–5864, Jun. 2021.

[19] H. Ju and R. Zhang, "Throughput maximization in wireless powered communication networks," *IEEE Trans. Wireless Commun.*, vol. 13, no. 1, pp. 418–428, Jan. 2014.

[20] Z. Chu, Z. Zhu, F. Zhou, M. Zhang, and N. Al-Dhahir, "Intelligent reflecting surface assisted wireless powered sensor networks for Internet of Things," *IEEE Trans. Commun.*, vol. 69, no. 7, pp. 4877–4889, Jun. 2021.

[21] M. Hua and Q. Wu, "Joint dynamic passive beamforming and resource allocation for IRS-aided full-duplex WPCN," *IEEE Trans. Wireless Commun.*, vol. 21, no. 7, pp. 4829–4843, Jul. 2022.

[22] Z. Wang, Y. Shi, Y. Zhou, H. Zhou, and N. Zhang, "Wireless-powered over-the-air computation in intelligent reflecting surface-aided IoT networks," *IEEE Internet Things J.*, vol. 8, no. 3, pp. 1585–1598, Feb. 2021.

[23] Y. Zheng, S. Bi, Y.-J. A. Zhang, X. Lin, and H. Wang, "Joint beamforming and power control for throughput maximization in IRS-assisted MISO WPCNs," *IEEE Internet Things J.*, vol. 8, no. 10, pp. 8399–8410, May 2021.

[24] S. Vijay and B. Chauhan, "Antenna miniaturization for IoT applications," in *Next-Generation Antennas: Advances and Challenges*. Hoboken, NJ, USA: Wiley, Jul. 2021, pp. 105–117.

[25] Z. Li, W. Chen, Q. Wu, H. Cao, K. Wang, and J. Li, "Robust beamforming design and time allocation for IRS-assisted wireless powered communication networks," *IEEE Trans. Commun.*, vol. 70, no. 4, pp. 2838–2852, Apr. 2022.

[26] S. Hu, Z. Wei, Y. Cai, C. Liu, D. W. K. Ng, and J. Yuan, "Robust and secure sum-rate maximization for multiuser MISO downlink systems with self-sustainable IRS," *IEEE Trans. Commun.*, vol. 69, no. 10, pp. 7032–7049, Oct. 2021.

[27] H. Li, W. Cai, Y. Liu, M. Li, Q. Liu, and Q. Wu, "Intelligent reflecting surface enhanced wideband MIMO-OFDM communications: From practical model to reflection optimization," *IEEE Trans. Commun.*, vol. 69, no. 7, pp. 4807–4820, Jul. 2021.

[28] S. Abeywickrama, R. Zhang, Q. Wu, and C. Yuen, "Intelligent reflecting surface: Practical phase shift model and beamforming optimization," *IEEE Trans. Commun.*, vol. 68, no. 9, pp. 5849–5863, Sep. 2020.

[29] W. Tang et al., "On channel reciprocity in reconfigurable intelligent surface assisted wireless networks," *IEEE Wireless Commun.*, vol. 28, no. 6, pp. 94–101, Dec. 2021.

[30] B. Zheng, C. You, W. Mei, and R. Zhang, "A survey on channel estimation and practical passive beamforming design for intelligent reflecting surface aided wireless communications," 2021, *arXiv:2110.01292*.

[31] Y. Lin, S. Jin, M. Matthaiou, and X. You, "Tensor-based algebraic channel estimation for hybrid IRS-assisted MIMO-OFDM," *IEEE Trans. Wireless Commun.*, vol. 20, no. 6, pp. 3770–3784, Jun. 2021.

[32] E. Boshkovska, R. Morsi, D. W. K. Ng, and R. Schober, "Power allocation and scheduling for SWIPT systems with non-linear energy harvesting model," in *Proc. IEEE Int. Conf. Commun. (ICC)*, May 2016, pp. 1–6.

[33] D. Tse and P. Viswanath, *Fundamentals of Wireless Communication*. Cambridge, U.K.: Cambridge Univ. Press, 2005.

[34] Y. Polyanskiy, H. V. Poor, and S. Verdú, "Channel coding rate in the finite blocklength regime," *IEEE Trans. Inf. Theory*, vol. 56, no. 5, pp. 2307–2359, May 2010.

[35] C. Sun, C. She, C. Yang, T. Q. Quek, Y. Li, and B. Vucetic, "Optimizing resource allocation in the short blocklength regime for ultra-reliable and low-latency communications," *IEEE Trans. Wireless Commun.*, vol. 18, no. 1, pp. 402–415, Jan. 2019.

[36] S. Boyd and L. Vandenberghe, *Convex Optimization*. Cambridge, U.K.: Cambridge Univ. Press, 2004.

[37] Z. Wang, T. Zhou, T. Xu, Y. Zhao, and H. Hu, "Capacity Characterization for reconfigurable intelligent surface aided MIMO communication under practical phase shift model," in *Proc. IEEE 32nd Annu. Int. Symp. Pers., Indoor Mobile Radio Commun. (PIMRC)*, Helsinki, Finland, Sep. 2021, pp. 1413–1418.

[38] T. M. Cover, *Elements of Information Theory*. New Delhi, India: Wiley, 1999.

Nan Cheng (Member, IEEE) received the B.E. and M.S. degrees from the Department of Electronics and Information Engineering, Tongji University, Shanghai, China, in 2009 and 2012, respectively, and the Ph.D. degree from the Department of Electrical and Computer Engineering, University of Waterloo, Waterloo, ON, Canada, in 2016.

He worked as a Postdoctoral Fellow with the Department of Electrical and Computer Engineering, University of Toronto, Toronto, ON, Canada, from 2017 to 2019. He is currently a Professor with the State Key Laboratory of ISN and the School of Telecommunications Engineering, Xidian University, Xi'an, Shaanxi, China. He has published over 70 journal papers in IEEE transactions and other top journals. His current research focuses on B5G/6G, space–air–ground integrated network, and self-driving system. His research interests also include AI-driven future networks.

Prof. Cheng serves as an Associate Editor for IEEE TRANSACTIONS ON VEHICULAR TECHNOLOGY, IEEE OPEN JOURNAL OF THE COMMUNICATIONS SOCIETY, and *Peer-to-Peer Networking and Applications*, and serves/served as a guest editor for several journals.
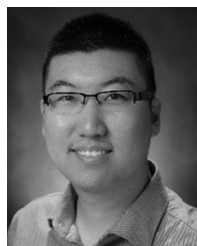
Ran Zhang (Senior Member, IEEE) received the B.Sc. degree in electrical and computer engineering from Tsinghua University, Beijing, China, in 2010, and the Ph.D. degree in electrical and computer engineering from the University of Waterloo, Waterloo, ON, Canada, in 2016.

He then joined the Ottawa Research Center, Huawei Technologies, Ottawa, ON, Canada, in 2016, as a System Engineer. He is currently an Assistant Professor with the Department of Electrical and Computer Engineering, Miami University, Oxford, OH, USA. His research interests include radio resource management for next-generation wireless communication networks, Internet of Things, channel coding for 5G New Radio, machine learning, unmanned aerial systems, robot-assisted e-healthcare, autonomous vehicular networks, and smart grid.

Dr. Zhang received the Best Paper Award from the IEEE GLOBECOM 2014, the CFR Faculty Research Award from Miami University in 2021, and the NSF Engineering Research Initiation Grant in 2022.

Ying Wang (Member, IEEE) received the Ph.D. degree in circuits and systems from Beijing University of Posts and Telecommunications (BUPT), Beijing, China, in 2003.

She is currently a Professor with BUPT, where she is also the Director of the Radio Resource Management Laboratory, Wireless Technology Innovation Institute. She is active in standardization activities of 3GPP and ITU. She took part in performance evaluation work of the Chinese Evaluation Group, as a Representative of BUPT. She has authored over 100 papers in international journals and conferences proceedings. Her research interests are in the area of the cooperative systems and radio resource management in wireless communications.

Prof. Wang was a recipient of the First Prize of the Scientific and Technological Progress Award by the China Institute of Communications in 2006 and 2009, respectively, and the Second Prize of the National Scientific and Technological Progress Award in 2008. She was also selected in the New Star Program of Beijing Science and Technology Committee and the New Century Excellent Talents in University, Ministry of Education, in 2007 and 2009, respectively.

Ruijin Sun (Member, IEEE) received the Ph.D. degree from Beijing University of Posts and Telecommunications, Beijing, China, in 2019.

She is currently a Lecturer with the School of Telecommunications Engineering and the State Key Laboratory of ISN, Xidian University, Xi'an, Shanxi, China. She worked as a joint Postdoctoral Fellow with Peng Cheng Laboratory, Shenzhen, China, and Tsinghua University, Beijing, from 2019 to 2021. She was a visiting student with the University of Waterloo, Waterloo, ON, Canada, from September 2017 to September 2018. Her research interests are in the area of knowledge-driven wireless resource allocation and MIMO signal processing.

Changle Li (Senior Member, IEEE) received the Ph.D. degree in communication and information system from Xidian University, Xi'an, China, in 2005.

He conducted his postdoctoral research in Canada and the National Institute of Information and Communications Technology, Tokyo, Japan, respectively. He had been a Visiting Scholar with the University of Technology Sydney, Ultimo, NSW, Australia. He is currently a Professor with the State Key Laboratory of Integrated Services Networks, Xidian University. His research interests include intelligent transportation systems, vehicular networks, mobile ad hoc networks, and wireless sensor networks.